Macrophage Innate Training Induced by IL-4 and IL-13 Activation Enhances OXPHOS Driven Anti-Mycobacterial Responses

Mimmi L. E. Lundahl[1,2]*, Morgane Mitermite[3a], Dylan G. Ryan[4,5a], Sarah Case[6], Niamh C. Williams[4], Ming Yang[5], Roisin I. Lynch[1], Eimear Lagan[7], Filipa Lebre[1], Aoife L. Gorman[1], Bojan Stojkovic[3], Adrian P. Bracken[7], Christian Frezza[5], Fred J. Sheedy[6], Eoin M. Scanlan[2], Luke A. J. O'Neill[4], Stephen V. Gordon[3], Ed C. Lavelle[1,8]*.

[1]School of Biochemistry and Immunology, Adjuvant Research Group, Trinity Biomedical Sciences Institute, Trinity College Dublin, Dublin, D02 R590 Ireland.

[2]School of Chemistry, Scanlan Research Group, Trinity Biomedical Sciences Institute, Trinity College Dublin, Dublin, D02 R590 Ireland.

[3]School of Veterinary Medicine, UCD Veterinary Sciences Centre, University College Dublin, Dublin, Ireland.

[4]School of Biochemistry and Immunology, Inflammation Research Group, Trinity Biomedical Sciences Institute, Trinity College Dublin, D02 R590 Ireland.

[5]Hutchison/MRC Research centre, MRC Cancer Unit, University of Cambridge, Cambridge, CB2 0XZ UK.

[6]School of Biochemistry and Immunology, Macrophage Homeostasis Group, Trinity Biomedical Sciences Institute, Trinity College Dublin, Dublin, D02 R590 Ireland.

[7]School of Genetics and Microbiology, Department of Genetics, Trinity College Dublin, Ireland.

[8]Lead contact

[a]Share joint second authorship

*Correspondence: lavellee@tcd.ie and lundahlm@tcd.ie

Abstract

Macrophages are a highly adaptive population of innate immune cells. Polarization with IFNγ and LPS into the "classically activated" M1 macrophage enhances pro-inflammatory and microbicidal responses, important for eradicating bacteria such as *Mycobacterium tuberculosis*. By contrast, "alternatively activated" M2 macrophages, polarized with IL-4, oppose bactericidal mechanisms and allow mycobacterial growth. These activation states are accompanied by distinct metabolic profiles, where M1 macrophages favor near exclusive use of glycolysis, whereas M2 macrophages up-regulate oxidative phosphorylation (OXPHOS). Here we demonstrate that activation with IL-4 and IL-13 counterintuitively induces protective innate memory against mycobacterial challenge. In human and murine models, prior activation with IL-4/13 enhances pro-inflammatory cytokine secretion in response to a secondary stimulation with mycobacterial ligands. In our murine model, enhanced killing capacity is also demonstrated. Despite this switch in phenotype, IL-4/13 trained murine macrophages do not demonstrate M1-typical metabolism, instead retaining heightened use of OXPHOS. Moreover, inhibition of OXPHOS with oligomycin, 2-deoxy glucose or BPTES all impeded heightened pro-inflammatory cytokine responses from IL-4/13 trained macrophages. Lastly, this work identifies that IL-10 attenuates protective IL-4/13 training, impeding pro-inflammatory and bactericidal mechanisms.

In summary, this work provides new and unexpected insight into alternative macrophage activation states in the context of mycobacterial infection.

Introduction

A significant feature of macrophages is dynamic plasticity, expressed by their ability to polarize towards distinct activation states (M. L. E. Lundahl, Scanlan, & Lavelle, 2017; Sica, Erreni, Allavena, & Porta, 2015). Activation with interferon gamma (IFNγ) together with lipopolysaccharides (LPS) yields the bactericidal and pro-inflammatory "classically activated" or M1 macrophages (Ferrante & Leibovich, 2012; Sica et al., 2015), whereas activation with the type 2 and regulatory cytokines, interleukin (IL)-4, IL-13, IL-10 and transforming growth factor (TGF)β, results in "alternatively activated" M2 macrophages, which enhance allergic responses, resolve inflammation and induce tissue remodeling (Bystrom et al., 2008; Mantovani et al., 2004). Another key difference between these activation states are their metabolic profiles: whereas classically activated macrophages switch to near exclusive use of glycolysis to drive their ATP production, alternatively activated macrophages instead upregulate their oxidative phosphorylation (OXPHOS) machinery (Van den Bossche et al., 2016; Van den Bossche, O'Neill, & Menon, 2017).

Macrophages are key host innate immune cells for controlling the causative agent of tuberculosis (TB), *Mycobacterium tuberculosis* (Cohen et al., 2018). *M. tuberculosis* has arguably caused the most deaths of any pathogen in human history and continues to be the cause of more than a million deaths annually: in 2020, 10 million people fell ill with active TB and 1.5 million died from the disease (World Health Organization, 2021). Whilst classifying macrophages into classical and alternative activation states is a simplification – the reality is a broad spectrum of various differentiation states that is continuously regulated by a myriad of signals (Sica et al., 2015) – it is nevertheless considered that for a host to control TB infection, classical macrophage activation is vital (Jouanguy et al., 1999; Philips & Ernst, 2012). Furthermore, a macrophage metabolic shift to glycolysis has been postulated to be a key for effective killing and thus overall control of TB infection (Gleeson et al., 2016; Huang, Nazarova, Tan, Liu, & Russell, 2018). By contrast, alternatively activated macrophages directly oppose bactericidal responses, which has been demonstrated to lead to enhanced bacterial burden and TB pathology (Moreira-Teixeira et al., 2016; Shi, Jiang, Bushkin, Subbian, & Tyagi, 2019). Due in part to the established ability of classically activated macrophages to kill *M. tuberculosis*, inducing Th1 immunity has been a key aim for TB vaccine development (Abebe, 2012; Andersen & Kaufmann, 2014; Ottenhoff et al., 2010). Apart from targeting adaptive immune

memory, another promising approach has emerged in recent years: bolstering innate immune killing capacity by the induction of innate training (Khader et al., 2019; Moorlag et al., 2020).

Innate training is regarded as a form of immunological memory. It is a phenomenon where a primary challenge, such as a vaccination or an infection, induces epigenetic changes in innate immune cells, which alters their responses following a secondary challenge (Arts et al., 2018; Saeed et al., 2014; van der Meer, Joosten, Riksen, & Netea, 2015). Unlike adaptive immune memory, the secondary challenge does not need to be related to the primary challenge. For instance, Bacille Calmette-Guérin (BCG) vaccination has been demonstrated to protect severe combined immunodeficiency (SCID) mice from lethal *Candida albicans* infection; reducing fungal burden and significantly improving survival (Kleinnijenhuis et al., 2012). This ability of the BCG vaccine to train innate immunity is now believed to be a mechanism by which it induces its protection against *M. tuberculosis*. Apart from the BCG vaccine, it has been demonstrated that other organisms and compounds can induce innate training, such as β-glucan (van der Meer et al., 2015) which induced protective innate training against virulent *M. tuberculosis*, as shown by enhanced mouse survival following *in vivo* infection, and enhanced human monocyte pro-inflammatory cytokine secretion following *ex vivo* infection (Moorlag et al., 2020).

Conversely, there is a risk that certain immune challenges could lead to innate immune re-programming that hinders protective immune responses. For instance, recent reports have demonstrated how virulent *M. tuberculosis* (N. Khan et al., 2020) and mycobacterial phenolic glycans (M. Lundahl et al., 2020) can program macrophages to attenuate bactericidal responses to subsequent mycobacterial challenge. In the current study, macrophage activation caused by former or concurrent parasitic infections is considered regarding the possibility of innate immune re-programming that hinders protective immune responses against this disease. Geographically, there is extensive overlap between tuberculosis endemic areas and the presence of helminths (Salgame, Yap, & Gause, 2013). With regard to macrophage activation and combatting tuberculosis, this is an issue as parasites induce type 2 responses, leading to alternative macrophage activation instead of classical activation and associated bactericidal responses (Chatterjee et al., 2017; X. X. Li & Zhou, 2013). Indeed, it was recently demonstrated how products of the helminth *Fasciola hepatica* can train murine macrophages for enhanced secretion of the anti-inflammatory cytokine IL-10 (Quinn et al., 2019).

Due to the relevance of macrophage plasticity for the control of mycobacterial infection, we primarily focused upon macrophage activation and training in this context. Unexpectedly, our data indicates that macrophage activation with IL-4 and IL-13 induces innate training that enhances pro-inflammatory and bactericidal responses against mycobacteria. Although murine macrophages trained with IL-4 and IL-13 resemble classically activated macrophages, we identify that they do not

adopt their typical metabolic profile, instead retaining heightened OXPHOS activity and notably lacking a dependency on glucose and glycolysis. Lastly, we identify IL-10 as a negative regulator of this innate training response, which may have obscured previous identification of this macrophage phenotype.

Results

Prior Alternative Activation Enhances Mycobacterial Killing

Macrophages are key immune cells for combatting *M. tuberculosis*. Upon infection, alveolar macrophages serve as the initial hosts of the intracellular bacterium (Cohen et al., 2018) and bactericidal responses of recruited monocyte-derived macrophages (MDM) are crucial for control and killing of *M. tuberculosis* (Huang et al., 2018). Overall, it has been highlighted that an early Th1 driven immune response is key to early eradication of *M. tuberculosis*, where classical activation of macrophages results in effective bactericidal action. However, a complicating factor is the occurrence of concurrent parasitic disease, which instead drives Th2 immunity and alternative macrophage activation, which in turn has been demonstrated to enhance TB pathology (Moreira-Teixeira et al., 2016). In this context, we sought to investigate how type 2 responses may induce innate memory, and how such memory could affect macrophage bactericidal properties.

To investigate the effect of IL-4 and IL-13 on macrophage acute and innate memory responses, an *in vitro* model of BCG infection was used. Murine bone marrow-derived macrophages (BMDMs) were stimulated with IL-4 and IL-13 (M(4/13)) on Day -1, followed by infection with BCG Denmark on either Day 0 or Day 6 (**Figure 1A**). On either day, the macrophages were exposed to roughly 30 bacteria per cell and after three hours extracellular bacteria were removed by washing and internalized bacteria were measured by colony forming units (CFUs), resulting in roughly 1-4 bacteria per cell, depending on the difference in uptake (**Figure 1B**). Internalized bacteria were measured by CFU (**Figure S1A**) at 27- and 51 hours post infection and killing capacity was determined as difference in CFU after the 3-hour time point (**Figure 1C**).

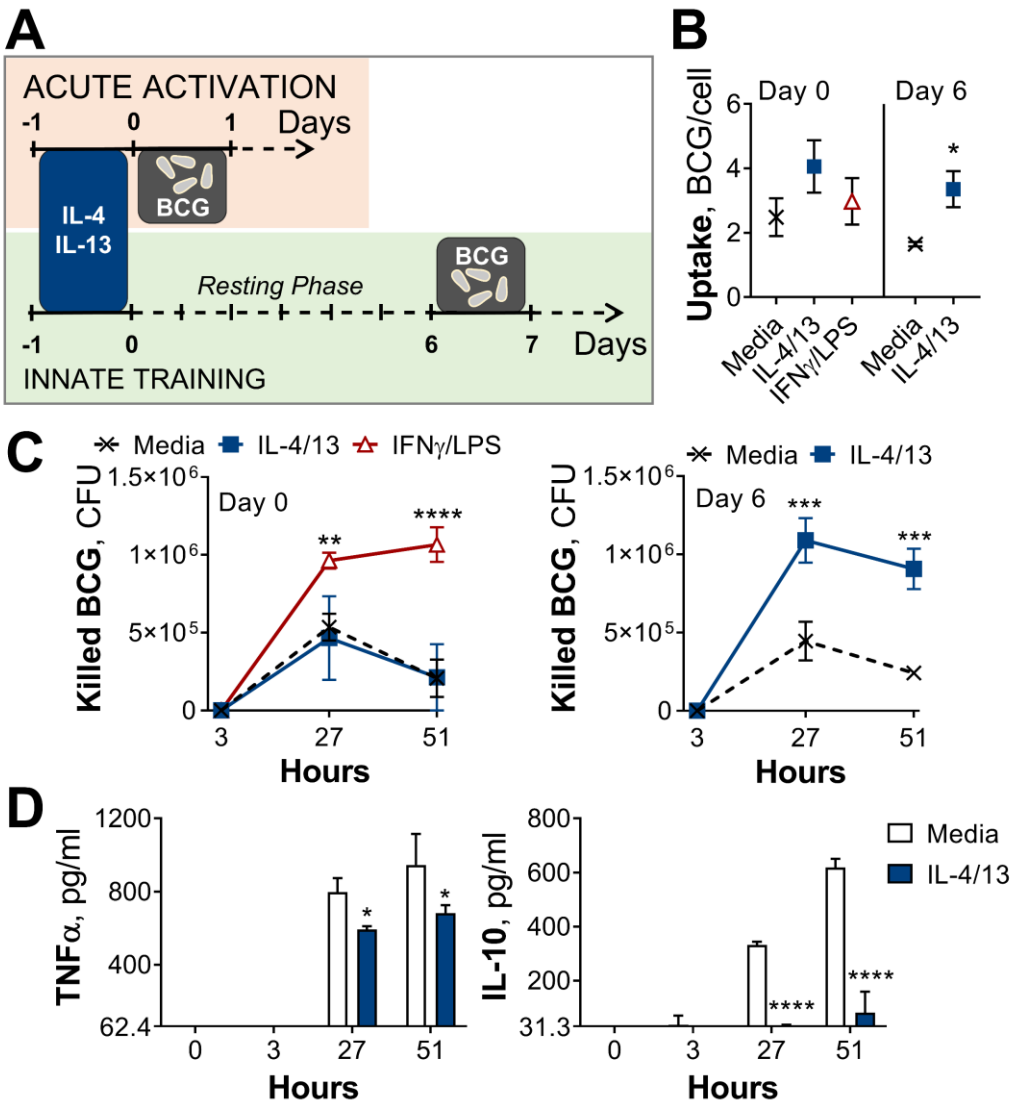

Figure 1. Training with IL-4 and IL-13 enhances BMDM mycobacterial killing capacity.

(**A**) Schematic of protocol for BCG infection following acute activation (Day 0) or training (Day 6) with IL-4 and IL-13. (**B-C**) BCG Denmark uptake (B) and killing after h as indicated (C), measured by difference in CFU after 3 hours per 0.5×10^6 BMDMs on Day 0 or Day 6. BMDMs were incubated with media, IL-4 with IL-13 or IFNγ with LPS for 24 h on Day -1. (**D**) Secretion of indicated cytokines from BMDMs treated as in (C), standardized to 0.5×10^6 BMDMs. (B-D) Representative results (n = 2 out of ≥ 3) showing mean ± SEM (B-C) or ± STD (D) and analyzed by student's t-test (B) or multiple t-tests, with Holm-Sidak correction (C-D), compared with media control. * $p \leq 0.05$, ** $p \leq 0.01$, **** $p \leq 0.0001$.

148 Mycobacterial killing was compared to naïve BMDMs incubated with media on day -1 (media control,
149 M(-)) on both Days 0 and 6, and BMDMs classically activated with IFNγ and LPS (M(IFNγ/LPS)) on Day
150 0. M(IFNγ/LPS) could not be investigated on Day 6 due to reduced viability: by Day 6, M(IFNγ/LPS)
151 displayed reduced cell numbers and upon the addition of live bacteria, all the remaining cells died
152 within 24 hours (not shown). On Day 0, M(IFNγ/LPS) displayed significantly enhanced mycobacterial
153 killing at 27- and 51-hours post infection, whereas M(4/13) displayed comparable killing capacity to
154 naïve M(-) (**Figure 1C**). Secretion of TNFα and IL-10 were also measured at 3-, 27- and 51 hours post
155 infection on Day 0 (**Figure S1B**) and Day 6 (**Figure 1D**). These cytokines were chosen as TNFα is critical
156 in the early host response against *M. tuberculosis* (Bourigault et al., 2013; Keane et al., 2001), while
157 IL-10 can prevent phagolysosome maturation in human macrophages (O'Leary, O'Sullivan, & Keane,
158 2011) and promote disease progression in mice (Beamer et al., 2008). Following BCG infection on Day
159 0 (**Figure S1B**), no IL-10 secretion was detected, and only bactericidal M(IFNγ/LPS) secreted detectable
160 levels of TNFα. Consistent with previous work, activation with IL-4 and IL-13 on the other hand did not
161 enhance BCG killing nor induce inflammatory cytokine secretion.
162 By contrast, on Day 6 (innate training responses), M(4/13) exhibited both heightened
163 mycobacterial uptake (**Figure 1B**) and significantly greater killing capacity compared with untrained
164 M(-), both at 27- and 51 hours post infection (**Figures 1C** and **S1A**). Furthermore, this was accompanied
165 by a near complete abrogation of IL-10 secretion, along with a minor decrease of TNFα compared with
166 M(-) (**Figure 1D**), displaying an overall shift towards a more pro-inflammatory response profile. To
167 investigate the change in phenotype of M(4/13) between the two days tested, a more detailed
168 characterization was carried out.
169
170 **Innate Training with IL-4 and IL-13 Promotes Pro-Inflammatory Responses**
171 The current dogma suggests that classical (M1) macrophage activation induces upregulation of
172 antigen presentation, enhanced secretion of pro-inflammatory cytokines including interleukin (IL)-1β,
173 IL-6 and TNFα, as well as the production of reactive oxygen and nitrogen species (ROS and RNS
174 respectively) (Bystrom et al., 2008; Sica et al., 2015). By contrast, alternatively activated macrophages
175 (M2) dampen inflammation, promote angiogenesis and scavenge debris (Gordon & Martinez, 2010;
176 Sica et al., 2015). These macrophages are identified by their upregulation of chitinase-like 3-1 (Chil3),
177 found in inflammatory zone-1 (Fizz1, Retnla) and arginase (Arg1) (Gabrilovich, Ostrand-Rosenberg, &
178 Bronte, 2012; Murray & Wynn, 2011), as well as surface expression of lectins, such as the macrophage
179 mannose receptor (MR, CD206) (Brown & Crocker, 2016). Flow cytometry and qPCR analysis of
180 M(IFNγ/LPS) and M(4/13), compared with inactivated M(-), showed that these activation phenotypes
181 tallied with the literature: M(IFNγ/LPS) had elevated expression of CD80, major histocompatibility
182 complex class II (MHC II) and inducible nitric oxide synthase (iNOS, *Nos2*) – responsible for production

183 of the reactive nitrogen species, nitric oxide (NO) – whereas M(4/13) exhibited heightened expression
184 of CD206, MHC II, *Arg1*, *Chil3* and *Retnla* (**Figures S2A-C**).
185 To examine their respective cytokine response profiles, M(IFNγ/LPS) and M(4/13) were
186 stimulated with killed *M. tuberculosis* strain H37Rv (hereafter referred to as Mtb) or the TLR1/2 ligand
187 tripalmitoyl-*S*-glyceryl-cysteine (PAM3CSK4) on either Day 0 or Day 6. Acutely activated M(IFNγ/LPS)
188 demonstrated elevated secretion of TNFα, IL-6 and IL-10 in response to Mtb (**Figure S2D**) and elevated
189 TNFα and IL-6 in response to PAM3CSK4 (**Figure S3A**), compared with M(-). By contrast, M(4/13) had
190 attenuated secretion of each cytokine compared with M(-), following either Mtb or PAM3CSK4
191 stimulation. However, on Day 6 (innate memory responses), both M(IFNγ/LPS) and M(4/13) secreted
192 greater pro-inflammatory TNFα and reduced anti-inflammatory IL-10 in response to Mtb (**Figure 2A**),
193 and secreted elevated TNFα following PAM3CSK4 stimulation (**Figure S3B**). M(4/13) additionally
194 exhibited increased IL-6 secretion in response to both stimuli. As with the BCG infection, M(IL-4/13)
195 responses changed markedly between Day 0 and Day 6, shifting towards a pro-inflammatory response
196 profile which was similar to classically activated macrophages.
197
198

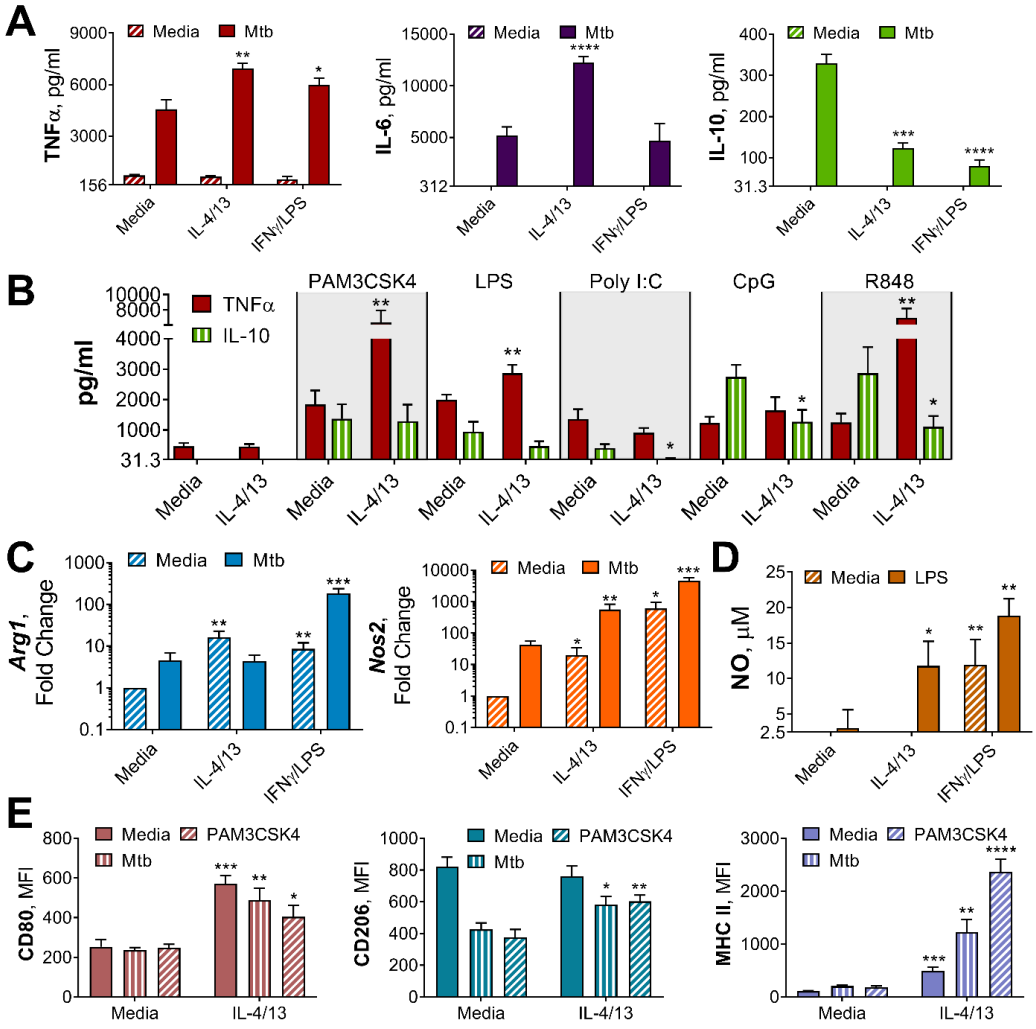

Figure 2. Innate training of BMDMs with IL-4 and IL-13 enhances pro-inflammatory responses.

(**A-B**) Cytokine secretion following BMDM 24 h incubation with irradiated *M. tuberculosis* (Mtb) (A), TLR agonists (B) or media on Day 6 as indicated. BMDMs were previously incubated with media, IL-4 with IL-13 or IFNγ with LPS on Day -1 for 24 h (n = 3). (**C**) qPCR of indicated mRNA in BMDMs treated as in (A), standardized to BMDMs incubated with media Day -1 and Day 6 (n = 4). (**D**) Nitric oxide (NO) secretion from BMDMs treated as in (B) (n = 3). (**E**) Expression of CD80, CD206 and MHC II (gating strategy Figure S2A) on BMDMs treated as in (A-B) (n = 3). Mean ± SD are shown and analyzed by student's t-test, compared with media control. * $p \leq 0.05$, ** $p \leq 0.01$, *** $p \leq 0.001$, **** $p \leq 0.0001$.

217 To consider whether the shift in M(4/13) to a pro-inflammatory cytokine profile was dependent on
218 epigenetic changes, the DNA methylation inhibitor 5'-deoxy-5'-(methylthio)adenosine (MTA), was
219 employed. This inhibitor has been demonstrated to impede training by BCG (Kleinnijenhuis et al.,
220 2012) and β-glucan (Quintin et al., 2012) – which promote pro-inflammatory responses – as well as
221 training induced by helminth *Fasciola hepatica* total extract (Quinn et al., 2019), which enhances anti-
222 inflammatory responses such as IL-10 and IL-1Ra secretion. The addition of MTA prior to activation
223 with IL-4 and IL-13 on day -1 reduced TNFα, IL-6 and IL-10 secretion induced by either Mtb or
224 PAM3CSK4 on Day 6 (**Figure S4A**), resulting in a profile reminiscent of acutely activated M(4/13)
225 (**Figure S2D**). By contrast, inhibition of DNA methylation in M(-) resulted in comparable or even
226 increased cytokine secretion. This suggested that DNA methylation following IL-4 and IL-13 activation
227 contributed to the innate training and subsequent enhancement of pro-inflammatory responses.
228 Moreover, in an attempt to identify which type of histone methylation was occurring, the following
229 global histone H3 modifications were investigated by western blot: H3K4me3, H3K27me3 and
230 H3K9me2 (**Figure S4 B-D**). Yeast β-glucan was used a positive control for innate training; however,
231 none of the tested conditions resulted in significant changes in global methylation at any of these
232 sites, demonstrating a need to investigate specific promoter regions in future studies.
233 Next, we addressed whether the shift towards pro-inflammatory responses was induced by
234 either IL-4 or IL-13 alone, or was induced by the two cytokines together, and moreover whether this
235 shift applicable to other stimuli. To address the former, BMDMs were trained with either IL-4, IL-13 or
236 both on Day -1, before incubation with media, Mtb or PAM3CSK4 on Day 6. It was observed that any
237 combination of IL-4 and IL-13 activation enhanced the secretion of TNFα in response to PAM3CSK4,
238 and that either IL-4 alone or IL-4 with IL-13 significantly reduced the secretion of IL-10 in response to
239 Mtb (**Figure S2E**). However, when comparing training with IL-4 alone or training with IL-4 and IL-13,
240 the combination of the two cytokines resulted further attenuation of IL-10 secretion, to a significant
241 extent, therefore the combination of the two cytokines continued to be used. To address whether
242 trained M(4/13) enhanced inflammatory responses was applicable to other stimuli, various Toll-like
243 receptor (TLR) agonists were employed on Day 6 (**Figure 2B**). Incubation of cells with ligands for
244 TLR1/2, TLR4, TLR7/8 or TLR 9 resulted in an increase of TNFα production, reduced IL-10 secretion or
245 both. This demonstrated that prior activation with IL-4 and IL-13 caused a subsequent shift towards a
246 pro-inflammatory response profile in response to a range of pathogen-related agonists.
247 Having considered cytokine responses, the expression of *Arg1* and *Nos2* and the secretion of
248 NO were next addressed. In mice, the induction of iNOS is important for bactericidal NO production
249 and subsequent killing of *M. tuberculosis* (Flynn et al., 1993; Pasula, Martin, Kesavalu, Abdalla, &
250 Britigan, 2017). In turn, Arg1 directly impedes the bactericidal function of iNOS by sequestering the

251 amino acid, arginine, which each enzyme uses to make their respective products: ornithine and NO.
252 Subsequently, in the murine model of TB infection, Arg1 has been linked with increased bacterial
253 burden and pathology (Moreira-Teixeira et al., 2016).

254 Without a secondary stimulation on Day 6, M(4/13) and M(IFNγ/LPS) displayed higher levels
255 of *Arg1* and *Nos2* expression, compared with BMDMs incubated in media alone (**Figure 2C**), and
256 M(IFNγ/LPS) exhibited markedly higher expression of *Nos2* compared with M(4/13). Following
257 stimulation with Mtb (**Figure 3C**) or PAM3CSK4 (**Figure S3C**) M(IFNγ/LPS) exhibited elevated
258 expression of both *Arg1* and *Nos2* compared with untrained M(-), however the trained M(4/13)
259 exhibited equivalent expression of *Arg1*, but with enhanced *Nos2*, demonstrating a further shift
260 towards an M1 profile. An increase in NO production could not be detected following Mtb stimulation;
261 however, following LPS stimulation, both M(4/13) and M(IFNγ/LPS) secreted greater levels of NO
262 compared to M(-) (**Figure 2D**).

263 Other M1 and M2 markers were analyzed by flow cytometry, following incubation with media,
264 Mtb or PAM3CSK4 on Day 6 (**Figure 2E**). Without secondary stimulation, M(4/13) exhibited an M1-
265 typical profile: heightened expression of CD80 and MHC II, whilst CD206 expression was comparable
266 to M(-). Following secondary stimulation with either Mtb or PAM3CSK4, M(4/13) CD80, CD206 and
267 MHC II expression was significantly greater compared with M(-). Having observed a change in
268 activation markers, cytokine induction and bactericidal capacity in M(4/13) between Days 0 and 6, the
269 next question was whether there was a corresponding shift in glycolytic metabolism.

270

271 **BMDMs Trained with IL-4 and IL-13 Retain OXPHOS Metabolism**

272 The increased energy and biosynthetic precursor demand induced by various macrophage activation
273 states are met in distinct ways. To demonstrate this, extracellular flux analysis was carried out, using
274 a mitochondrial stress test. Following basal respiration, oligomycin – an ATP synthase inhibitor – was
275 added to impede electron transport chain (ETC)-driven ATP synthesis, followed by the proton
276 ionophore FCCP (carbonyl cyanide-p-trifluoromethoxyphenylhydrazone), which uncouples the ETC
277 from ATP synthase, allowing maximal respiration, and lastly rotenone and antimycin-A were added,
278 which impede complex I and III of the ETC respectively. Consistent with previous studies, M(4/13) on
279 Day 1 displayed both an increase of oxygen consumption rate (OCR) – indicative of mitochondrial
280 OXPHOS activity – and extracellular acidification rate (ECAR) – an indirect measurement of lactic acid
281 secretion and thus indicative of glycolysis (**Figure 3A**). This demonstrated how alternative activation
282 is intrinsically linked with enhanced mitochondrial OXPHOS activity, via the tricarboxylic acid (TCA)
283 cycle (Van den Bossche et al., 2016; Wang et al., 2018). The TCA cycle is in turn driven by glycolysis,
284 glutaminolysis and fatty acid oxidation (Viola, Munari, Sánchez-Rodríguez, Scolaro, & Castegna, 2019).

285 By contrast, acutely activated M(IFNγ/LPS) displayed an increase in ECAR and reduced OCR (**Figure**
286 **3A**), which was indicative of augmented glycolysis to meet the increased need for ATP, whilst ATP
287 synthesis via OXPHOS is hindered (Liu et al., 2016). This glycolytic shift is critical for pro-inflammatory
288 responses induced by classically activated macrophages and moreover results in mitochondrial
289 dysfunction (Van den Bossche et al., 2016).
290
291
292
293
294
295
296
297
298
299
300

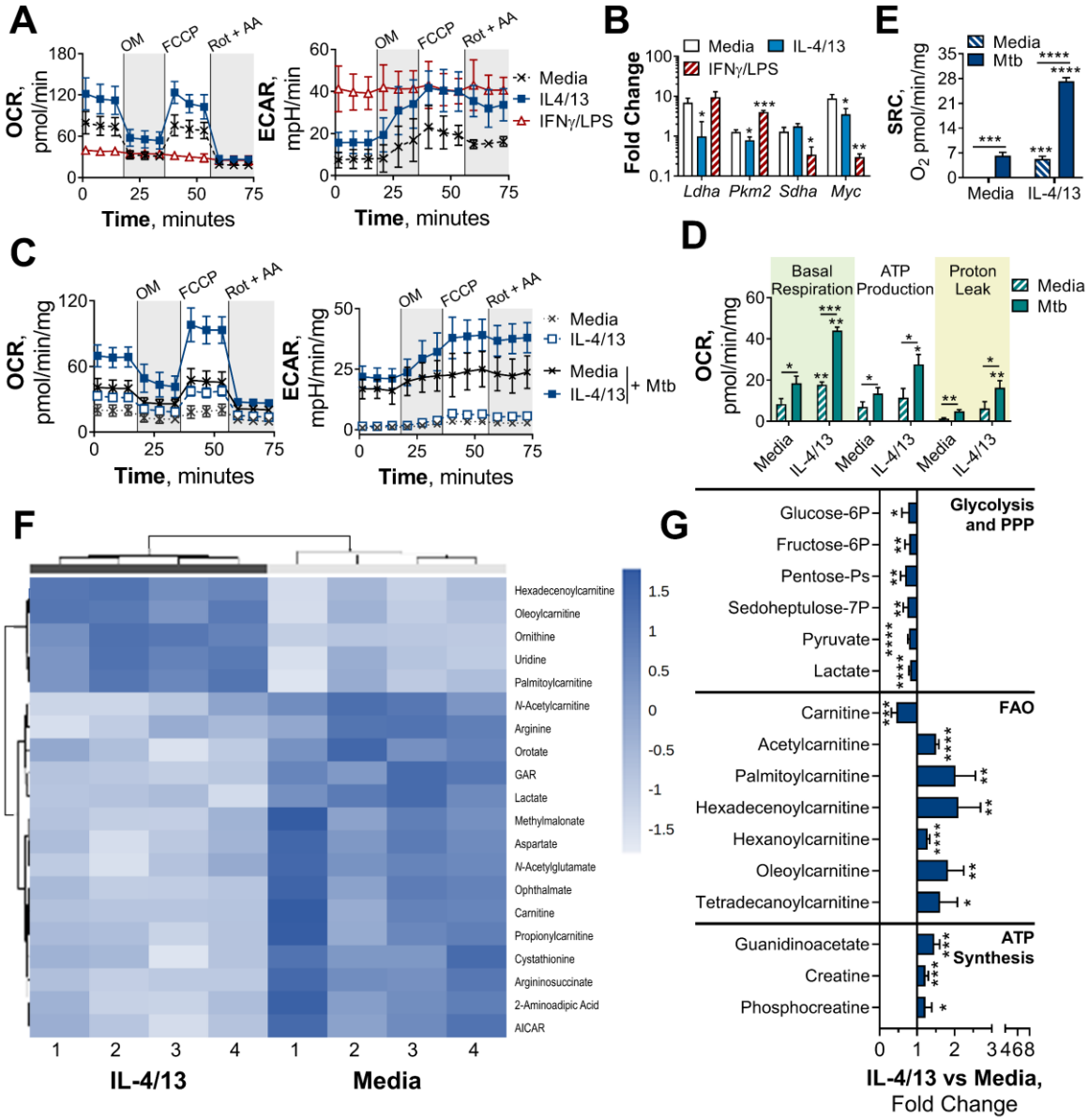

Figure 3. BMDMs trained with IL-4 and IL-13 retain M2-typical metabolism upon mycobacterial challenge.

(**A**) Extracellular flux analysis of BMDMs, following 24 h incubation with IL-4 and IL-13, IFNγ and LPS or media (n = 3). Mitochondrial stress test inhibitors: oligomycin (OM; blocks ATP synthase), FCCP (uncouples the electron transport chain [ETC] from ATP synthesis), rotenone (Rot; inhibits complex I of the ETC) and antimycin-A (AA; inhibits complex III of the ETC). (**B**) qPCR of indicated mRNA in BMDMs following incubation with media, IL-4 with IL-13 or IFNγ with LPS for 24 h on Day -1 and stimulated with irradiated *M. tuberculosis* (Mtb) for 6 h (*Pkm2*) or 24 h (*Ldha*, *Sdha* and *Myc*), standardized to BMDMs given media on Day -1 and Day 6 (n = 3). (**C-E**) Extracellular flux analysis (C), basal respiration, ATP production, proton leak (D) and spare respiratory capacity (SRC) (E) of BMDMs treated as in (B), with incubation with media or IL-4 with IL-13 on Day -1 and stimulation with media or Mtb for 24 h on Day 6 (n = 3). (**F-G**) Metabolites from BMDMs treated as in (B), incubated with media or IL-4 with IL-13 on Day -1 and stimulation with Mtb for 24 h on Day 6 (n = 4). MetaboAnalyst generated heatmap representing hierarchical clustering of the top 20 most up/down regulated metabolites (F). Fold change compared with media control (=1) (G). Mean ± SD are shown and analyzed by student's t-test. * $p \leq 0.05$, ** $p \leq 0.01$, *** $p \leq 0.001$, **** $p \leq 0.0001$. Abbreviations: AICAR, aminoimidazole carboxamide ribonucleotide; ECAR, extracellular acidification rate; FAO, fatty acid oxidation; GAR, glycinamide ribonucleotide; OCR, oxygen consumption rate; P, phosphate; PPP, pentose phosphate pathway.

319 Due to the link between glycolysis and classical activation, it is not surprising that prior work has
320 proposed that a macrophage glycolytic shift is crucial for effective killing and thus overall control of
321 TB infection (Gleeson et al., 2016; Huang et al., 2018). Furthermore, it has recently been proposed
322 that *M. tuberculosis* impedes this glycolytic shift as an immune evasion strategy (Hackett et al., 2020).
323 As we had observed that innate memory responses induced by IL-4 and IL-13 caused a switch towards
324 a pro-inflammatory and bactericidal response profile, akin to a classically activated macrophage, it
325 was pertinent to address whether there was an accompanying glycolytic shift. Previous work by Van
326 den Bossche et al. has highlighted that because IL-4 activated human MDMs retain their metabolic
327 versatility, they are able to be "re-polarized" to a classical phenotype (Van den Bossche et al., 2016).
328 This was demonstrated by activating MDMs for 24 hours with IL-4, before the cells were washed and
329 re-stimulated with IFNγ and LPS for another 24 hours. MDMs previously activated with IL-4 secreted
330 higher concentrations of TNFα, IL-6 and IL-12 compared with MDMs that were naïve prior to IFNγ and
331 LPS stimulation. This adaptive quality to re-polarize is restricted to alternatively activated
332 macrophages, as mitochondrial dysfunction in classically activated macrophages prevents them from
333 re-polarizing to an alternative phenotype (Van den Bossche et al., 2016). Subsequently, we next
334 addressed whether the IL-4 trained macrophages were adopting a metabolic profile similar to a
335 classical macrophage, or retaining their more versatile metabolic profile.

336 As with the BCG infection studies, due to the reduced viability (as observed by reduced cell
337 numbers over time) of the M(IFNγ/LPS) by Day 6 and 7, OCR and ECAR measurements did not reach
338 the detection limit. To compare metabolic phenotypes of the trained macrophages at these later time
339 points, transcription profiles were therefore analyzed. Prior work has established that the
340 transcription factor hypoxia-inducible factor-1 alpha (HIF-1α) aids the glycolytic metabolic shift
341 following classical activation, such as upregulating the enzyme lactate dehydrogenase (LDH) (Seth et
342 al., 2017) to increase lactic acid fermentation. Tallying with these studies, trained M(IFNγ/LPS) on Day
343 7 exhibited elevated expression of LDH (*Ldha*) and pyruvate kinase isozyme M2 (PKM2, *Pkm2*) (**Figure**
344 **S5A**). PKM2 has been shown to play a key role in stabilizing HIF-1α and is thus a crucial determinant
345 for glycolytic metabolism re-wiring (Palsson-McDermott et al., 2015). By contrast, on Day 7, M(4/13)
346 displayed a similar level of LDH expression and reduced transcription of PKM2 compared with M(-).

347 On the other hand, considering OXPHOS machinery at this time point, trained M(IFNγ/LPS)
348 showed reduced expression of the TCA cycle enzyme succinate dehydrogenase (SDH, *Sdha*), whereas
349 this downregulation was not present in M(4/13) (**Figure S5A**). Moreover, M(4/13) and M(IFNγ/LPS)
350 respectively displayed increased and decreased expression of the transcription factor
351 myelocytomatosis viral oncogene (c-Myc, *Myc*). IL-4 and IL-13 induce c-Myc expression in alternatively
352 activated macrophages (L. Li et al., 2015; Luiz et al., 2020) and contrastingly LPS induced upregulation

353 of HIF-1α occurs in tandem with downregulation of c-Myc (Liu et al., 2016). Overall, without secondary
354 stimulation, both trained M(IFNγ/LPS) and M(4/13) retained transcriptional and metabolic profiles
355 consistent with previous reports.

356 Upon secondary stimulation on Day 6 with either Mtb (**Figure 3B**) or PAM3CSK4 (**Figure S5B**),
357 M(IFNγ/LPS) maintained the elevated expression of *Pkm2*, accompanied by reduced transcription of
358 *Sdha* and *Myc*. *Myc* expression was induced in untrained M(-) and M(4/13) by both secondary stimuli,
359 although Mtb did not enhance *Myc* in M(4/13) to the same extent as M(-). Regarding glycolytic
360 metabolism, M(4/13) displayed relatively reduced *Ldha* upon Mtb incubation (**Figure 3B**) and further
361 maintained a similar level of *Sdha* compared with M(-). These results indicated that trained
362 M(IFNγ/LPS) and M(4/13) maintained their respective metabolic profiles following secondary
363 stimulation with Mtb or PAM3CSK4. As such, these results indicated again that trained M(IFNγ/LPS)
364 and M(IL-4/13) maintained their respective metabolic profiles following secondary stimulation with
365 Mtb or PAM3CSK4.

366 That trained M(4/13) retain OXPHOS metabolism was furthermore supported by Mtb
367 stimulation increasing both OCR and ECAR in M(-) and M(4/13) (**Figure 3C**), where M(4/13) displayed
368 significantly greater OXPHOS driven basal respiration, ATP production and concomitant proton
369 leakage compared with M(-) (**Figure 3D**). In addition, in response to either Mtb (**Figure 3E**) or
370 PAM3CSK4 (**Figure S5C**) there was an increase in spare respiratory capacity (SRC), further signifying
371 that trained M(4/13) retain and even elevate OXPHOS metabolism following secondary stimulation
372 with Mtb.

373 To further investigate the metabolic profile of trained M(IL-4/13) vs untrained (media control)
374 stimulated with Mtb, the relative change of intracellular metabolite abundance was furthermore
375 assessed by liquid chromatography-mass spectrometry (LC-MS, **Figures 3F-G** and **S5D-E**). This semi-
376 targeted analysis revealed that the trained M(4/13) appeared to have increased use of the urea cycle,
377 as shown by reduced aspartate, arginine and argininosuccinate levels along with enhanced ornithine
378 (**Figure S5E**). Furthermore, there were reduced levels of metabolites associated with glycolysis and
379 the pentose phosphate pathway (PPP) – such as lactate and sedoheptulose-7-phosphate – whilst
380 metabolites involved in fatty acid oxidation (FAO) and ATP synthesis regulation were enhanced (**Figure
381 3G**). In the case of FAO, reduced carnitine with enhanced carnitine-bound fatty acids (acyl carnitines)
382 signified that fatty acids were being ferried by carnitine into the mitochondrion for FAO. FAO is
383 upregulated during murine M2 macrophage activation and results in the production of acetyl-CoA,
384 NADH and $FADH_2$, which are further used to fuel the TCA cycle and downstream OXPHOS (O'Neill,
385 Kishton, & Rathmell, 2016). Furthermore, the upregulation of creatine and phosphocreatine – as well
386 as creatine biosynthesis precursor guanidinoacetate – intimated enhanced ATP synthesis. Creatine

387 reacts with ATP to form ADP and phosphocreatine, transporting ATP out of the mitochondrion and
388 preventing allosteric inhibition of ATP synthesis. In the trained M(4/13) the amount of
389 phosphocreatine per ATP was enhanced (**Figure S5F**), which indicated enhanced mitochondrial ATP
390 synthesis and supported the hypothesis that OXPHOS was enhanced. Overall, these results suggested
391 the trained M(4/13) were upregulating their OXPHOS activity in response to mycobacterial challenge.
392 Having observed that trained M(IL-4/IL-13) showed a distinct metabolic profile from classically
393 activated macrophages, the roles of glycolysis and OXPHOS in driving cytokine production were next
394 investigated with the use of inhibitors. Incubation with the glycolysis and OXPHOS inhibitor 2-deoxy
395 glucose (2-DG) (Wang et al., 2018) prior to stimulation with Mtb (**Figure S6A**) significantly reduced
396 TNFα secretion in M(IFNγ/LPS) and M(-). 2-DG also reduced PAM3CSK4 induced TNFα in M(4/13) and
397 M(IFNγ/LPS) (**Figure S6B**) and reduced IL-6 secretion in M(4/13) following either Mtb or PAM3CSK4
398 stimulation. Secretion of anti-inflammatory IL-10 following Mtb stimulation was also reduced by 2-DG
399 in M(IFNγ/LPS) and M(4/13). This demonstrated that glycolysis, OXPHOS or both were involved in
400 driving cytokine responses to Mtb and PAM3CSK4 in all tested macrophages.
401 To further examine the role of OXPHOS, the ATP-synthase inhibitor oligomycin (OM) and the
402 glutaminase inhibitor bis-2-(5-phenylacetamido-1,3,4-thiadiazol-2-yl)ethyl sulfide (BPTES) were used
403 prior to secondary stimulation. The role of glutaminolysis in the trained M(IL-4/13) was of interest, as
404 it has previously been highlighted to compensate for inhibition of glycolysis and fuel the TCA cycle
405 during IL-4 induced macrophage activation (Wang et al., 2018). In the trained M(4/13), inhibition of
406 either OXPHOS or glutaminolysis significantly reduced TNFα and IL-6 secretion following stimulation
407 with either Mtb (**Figure 4A**) or PAM3CSK4 (**Figure S6B**), suggesting that both processes helped drive
408 pro-inflammatory responses. By contrast, in trained M(IFNγ/LPS), although the markedly lower level
409 of IL-6 was further impeded by either inhibitor, the secretion of TNFα was unaffected, supporting
410 M(IFNγ/LPS) use of glycolysis to drive pro-inflammatory responses. OM and BPTES furthermore
411 impeded IL-10 secretion from M(IFNγ/LPS), whereas OM reduced IL-10 secretion in M(4/13) and
412 BPTES did not (**Figure 4A**). In the case of trained M(4/13) this implicated that glutamine metabolism
413 was selectively a driver of pro-inflammatory cytokine responses.
414

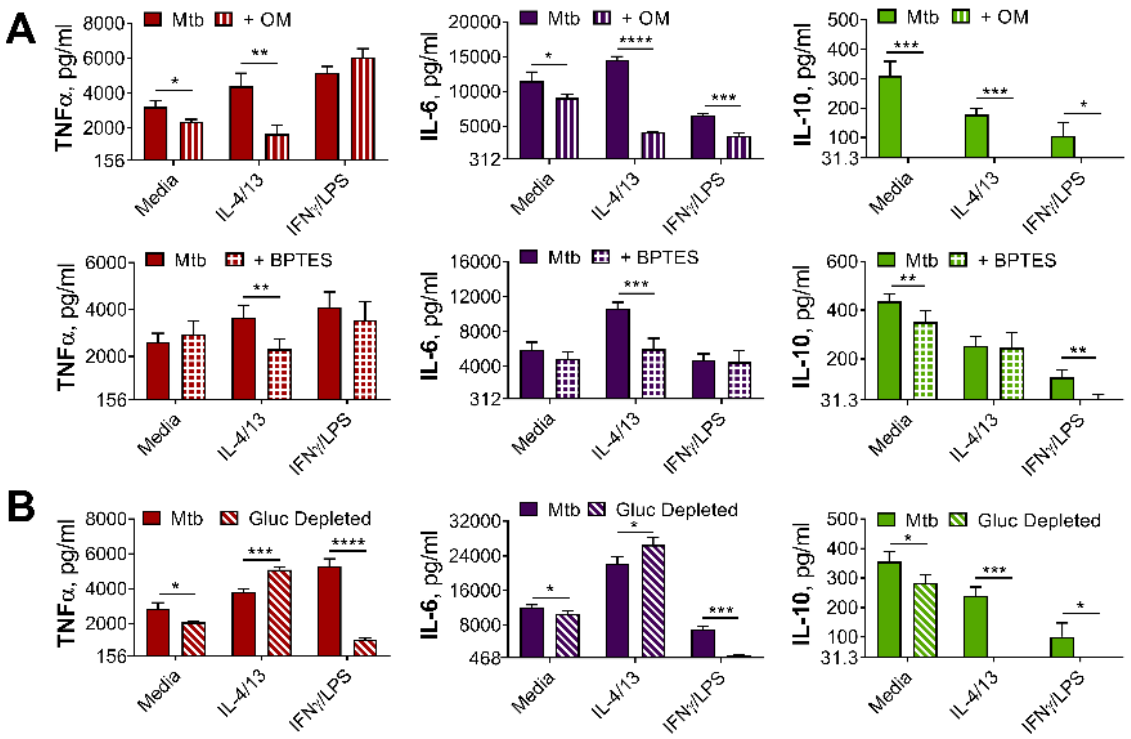

415

416 **Figure 4. OXPHOS drives inflammatory cytokine responses in IL-4/13 trained BMDMs.**

417 (**A**) Cytokine secretion from BMDMs following incubation with media, IL-4 with IL-13 or IFNγ with LPS for 24 h
418 on Day -1 and incubation with irradiated *M. tuberculosis* (Mtb) on Day 6 for 24 h, with or without pre-incubation
419 (Day 6) of oligomycin (OM) or BPTES (n = 4). (**B**) Cytokine secretion from BMDMs treated as in (A), with or without
420 glucose depleted conditions between Day -1 to 7 (n = 3). Mean ± SD are shown and analyzed by student's t-test
421 as indicated. * $p \leq 0.05$, ** $p \leq 0.01$, *** $p \leq 0.001$, **** $p \leq 0.0001$.

422

423

424

425

426

427

428

429

430

431

432

433

434

435

436

437

438

439 To further cement the differences in glycolytic metabolism between trained M(IFNγ/LPS) and M(4/13),
440 an experiment was carried out where BMDMs were incubated in either glucose depleted media or
441 regular glucose-rich media (both without pyruvate) from Day-1 (**Figure 4B**). Whereas glucose
442 depletion significantly reduced the secretion of TNFα, IL-6 and IL-10 from M(IFNγ/LPS) and M(-),
443 following Mtb stimulation on Day 6, glucose depletion did not impair pro-inflammatory cytokine
444 secretion of M(4/13); instead the secretion of both TNFα and IL-6 was elevated under these
445 conditions, whilst levels of regulatory IL-10 were further reduced, displaying an even greater shift
446 towards pro-inflammatory responses. Furthermore, stimulation with PAM3CSK4 yielded similar
447 results (**Figure S6C**), although IL-6 secretion remained unaltered. This highlighted that although
448 trained M(IFNγ/LPS) and M(4/13) had similar response profiles, M(4/13) appeared to retain M2-
449 typical metabolism (**Figure 5**).

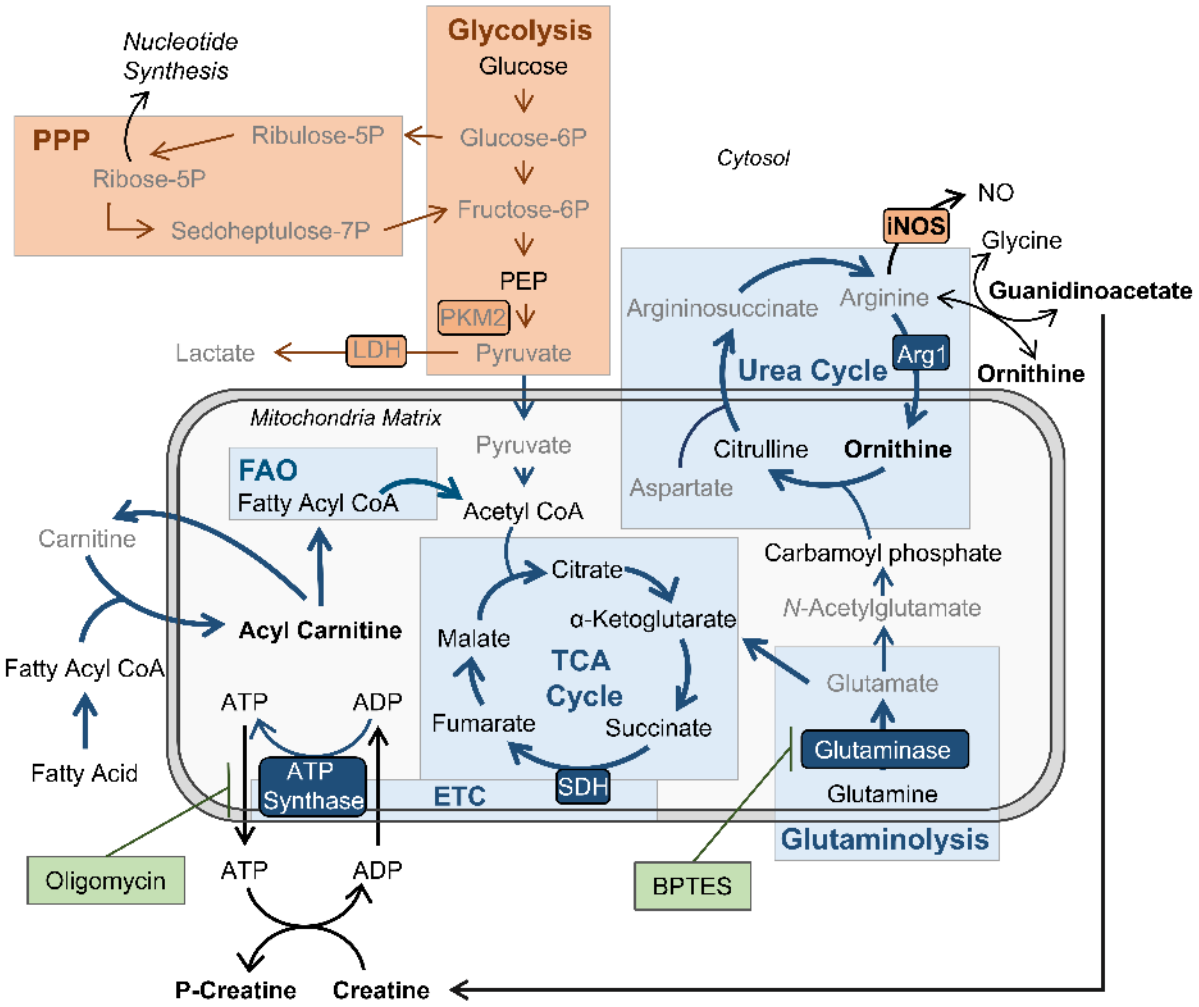

Figure 5. BMDMs trained with IL-4 and IL-13 retain M2-typical metabolism: schematic summary of results.

Pathways have been simplified. Key: metabolic pathways strongly upregulated by M1/M2 macrophage activation are highlighted by red/blue colored boxes, respectively. Inhibitors are indicated by green boxes. Arrow width represents which pathways are implicated (thicker) or not (narrower) in trained M(4/13) following stimulation with irradiated *M. tuberculosis* (Mtb). Metabolites (measured by LC-MS) or enzymes (measured by qPCR) written in bold or in grey text are enhanced or reduced respectively compared with untrained macrophages. Trained M(4/13) do not employ classical activated macrophage metabolism – aerobic glycolysis and pentose phosphate pathway (PPP) – and instead employ alternative activated macrophage metabolism, characterized by production of ATP through the tricarboxylic acid (TCA) cycle, coupled with the electron transport chain (ETC) via oxidative phosphorylation (OXPHOS), as well as enhanced use of the urea cycle. Glutaminolysis, FAO and ATP synthesis regulation are implicated. This is demonstrated by inhibitor experiments and by changed expression of metabolites. Abbreviations: LDH, lactate dehydrogenase; NO, nitric oxide; P, phosphate; PEP, Phosphoenolpyruvic acid; PKM2, pyruvate kinase M2; SDH, succinate dehydrogenase.

470 **IL-10 Negatively Regulates Innate Training**

471 A key consideration regarding alternative macrophage activation and TB infection is the influence of
472 concurrent parasitic disease. Along with IL-4 and IL-13, parasites can induce production of the
473 regulatory cytokine IL-10 (Gause, Wynn, & Allen, 2013; Roy et al., 2018), which moreover promotes
474 alternative macrophage activation (Bystrom et al., 2008; Mantovani et al., 2004). Furthermore, it has
475 been shown that products of the helminth *F. hepatica* can train macrophages to secrete more IL-10
476 following secondary LPS stimulation (Quinn et al., 2019). Given its association with alternative
477 macrophage activation and parasitic infection, we next considered the potential role of IL-10 in IL-
478 4/13 induced macrophage innate memory responses.

479 BMDMs were activated with IL-4, IL-13 and IL-10 (M(4/13/10)) to compare how this
480 phenotype may have differed from M(4/13). Following secondary stimulation with Mtb, both M(4/13)
481 and M(4/13/10) secreted lower concentrations of TNFα, IL-6 and IL-10 than M(-) on Day 1 (**Figure S7A**).
482 However, whilst M(4/13) demonstrated elevated TNFα and IL-6 by Day 7 (**Figure 6A**), inflammatory
483 cytokine secretion by M(4/13/10) was reduced on both Day 1 and Day 7. Furthermore, following acute
484 activation, M(4/13/10) had similarly elevated levels of *Arg1* as M(4/13) and a comparably minor
485 induction of *Nos2* (**Figure 6B**). The addition of IL-10 moreover caused even greater augmentation of
486 M2-associated *Chil3* and *Retnla* expression. Accompanying flow cytometry analysis demonstrated that
487 both M(4/13/10) and M(4/13) exhibited reduced expression of CD80, compared with M(-), along with
488 enhanced expression of CD206, where the M(4/13/10) had greater CD206 expression (**Figure S7B**).
489 Regarding MHC II, only M(4/13) displayed enhanced expression compared with M(-). The similar
490 upregulation of M2-characteristic markers indicated that M(4/13) and M(4/13/10) were two types of
491 alternatively activated macrophages.

492 A similar comparison was made at Day 7, where both M(4/13) and M(4/13/10) retained
493 enhanced *Arg1*, *Retnla* and *Chil3* expression and displayed enhanced *Nos2* expression compared with
494 naïve M(-) (**Figure S7C**). Regarding accompanying CD80, CD206 and MHC II expression (**Figure S7D**): in
495 all tested conditions, CD206 expression was comparable between M(4/13) and M(4/13/10), whereas
496 CD80 expression was elevated in M(4/13/10). Furthermore, M(4/13) retained an elevated expression
497 of MHC II, which increased two- and four-fold following stimulation with Mtb and PAM3CSK4,
498 respectively, whereas this elevation did not occur to the same degree in M(4/13/10). Whilst both
499 M(4/13) and M(4/13/10) moreover displayed similar expression of *Arg1* following Mtb stimulation on
500 Day 7, the addition of IL-10 during activation hindered the upregulation of *Nos2* observed in trained
501 M(4/13), and further enhanced the transcription of *Retnla and Chil3* (**Figure S7E**).

502

503

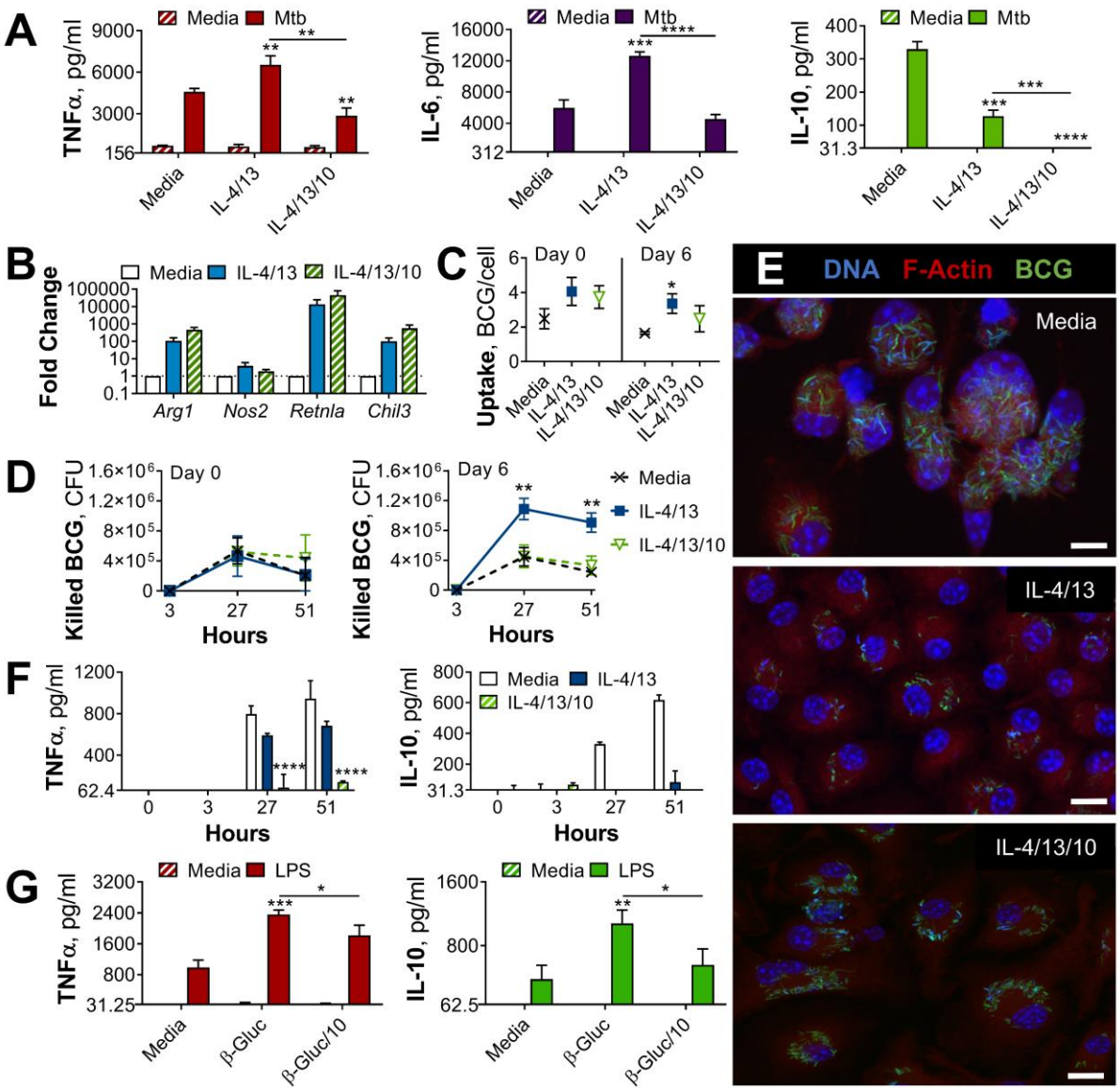

Figure 6. IL-10 inhibits bactericidal and pro-inflammatory training induced by IL-4 and IL-13 and alters yeast β-glucan training.

(**A**) Cytokine secretion following BMDM incubation with media or IL-4 and IL-13, with or without IL-10, for 24 h on Day -1 and incubated for 24 h with media or irradiated *M. tuberculosis* (Mtb) on Day 6. (**B**) qPCR of indicated mRNA in BMDMs following 24 h incubation with media or IL-4 and IL-13, with or without IL-10, standardized to media control (n=4). Mean ± SD are shown. (**C-F**) BCG Denmark uptake (C) killing after h as indicated (D) as measured by difference in CFU after 3 hours per 0.5×10^6 BMDMs on Day 0 or Day 6. Representative images of Hoechst- (blue), modified auramine-O- (green) and phalloidin (red)-stained BMDMs were taken on Day 6, 27 h after BCG incubation (E). Cytokine secretion on Day 6, at h indicated (F). BMDMs were previously incubated with media or IL-4 and IL-13, with or without IL-10, for 24 h on Day -1. (C-D, F) representative results (n = 2 of ≥ 3) are shown as mean ± SD (C, F) or SEM (D) and analyzed by student's t-test compared with media (C) or multiple t-tests, with Holm-Sidak correction, comparing with or without IL-10 (D, F). (**G**) Cytokine secretion following BMDM incubation with media or β-glucan (β-Gluc), with or without IL-10, for 24 h on Day -1 and incubated for 6 h (TNFα) or 24 h (IL-10) with media or LPS on Day 6. (A, G) Mean ± SD (n = 3) are shown and analyzed by student's t-test. * $p \leq 0.05$, ** $p \leq 0.01$, **** $p \leq 0.0001$.

523

524

525 Our next question was how the addition of IL-10 during alternative activation would affect
526 mycobacterial killing capacity. The BMDMs were incubated with roughly 30 BCG per cell on Day 0 or
527 Day 6. There were some differences in bacterial uptake (**Figure 6C**), where M(4/13) took up more
528 bacteria per cell on Day 6. Difference in CFU counts after the 3-hour time point (**Figure S1C**) were used
529 to calculate killing of internalized BCG. On Day 0, M(-), M(4/13) and M(4/13/10) displayed comparable
530 killing capacity (**Figure 6D**). Moreover, BCG infection did not induce detectable levels of TNFα or IL-10
531 (**Figure S1D**). On Day 6, M(-) and M(4/13/10) maintained a similar level of BCG killing, whereas M(4/13)
532 displayed enhanced bactericidal capacity. This indicated that IL-10 hindered the enhanced bactericidal
533 response induced by prior IL-4 and IL-13 macrophage activation. The difference in bacterial killing
534 capacity was further supported by confocal microscopy 27 hours after infection, where it was
535 observed that M(-) and M(4/13/10) had markedly more bacteria per cell compared with M(4/13)
536 (**Figure 6E**). Furthermore, whereas M(4/13) showed a shift towards pro-inflammatory cytokine
537 secretion, with IL-10 secretion being reduced whilst TNFα production was largely intact, M(4/13/10)
538 secreted significantly less TNFα than M(4/13), whilst IL-10 secretion was not enhanced (**Figure 6F**).
539 This would indicate that IL-10 regulated the training induced by IL-4 and IL-13, preventing both the
540 enhancement of killing capacity and the accompanying pro-inflammatory cytokine profile.
541 As IL-10 appeared to impede innate training induced by IL-4 and IL-3, the question of whether
542 IL-10 would impede training induced by other stimuli was investigated. BMDMs were trained with
543 yeast β-glucan – with or without the addition of IL-10 – prior to LPS stimulation a week later (**Figure**
544 **6G**). The addition of IL-10 during training reduced the enhanced secretion of both TNFα and IL-10,
545 demonstrating that IL-10 modulates innate training induced by other training stimuli, not only those
546 induced by IL-4 and IL-13.

547

548 **IL-4 and IL-13 Induced Training in Human Macrophages**

549 Having identified that trained murine M(IL-4/13) show enhanced inflammatory responses following
550 secondary challenge and that this was negatively regulated by IL-10, it was important to test whether
551 these findings were applicable to humans. Human monocyte-derived macrophages (MoDM) were
552 activated with human IL-4 and IL-13, with or without the addition of human IL-10 for 24 hours on Day
553 -1, and then challenged with irradiated Mtb (**Figure 7**) or PAM3CSK4 (**Figure S8**) on Day 0 (acute
554 activation) or Day 6 (innate training). MoDM incubated with media was used as a naïve/untrained
555 control and macrophages activated with human IFNγ and LPS were used to induce classical/M1
556 activation.

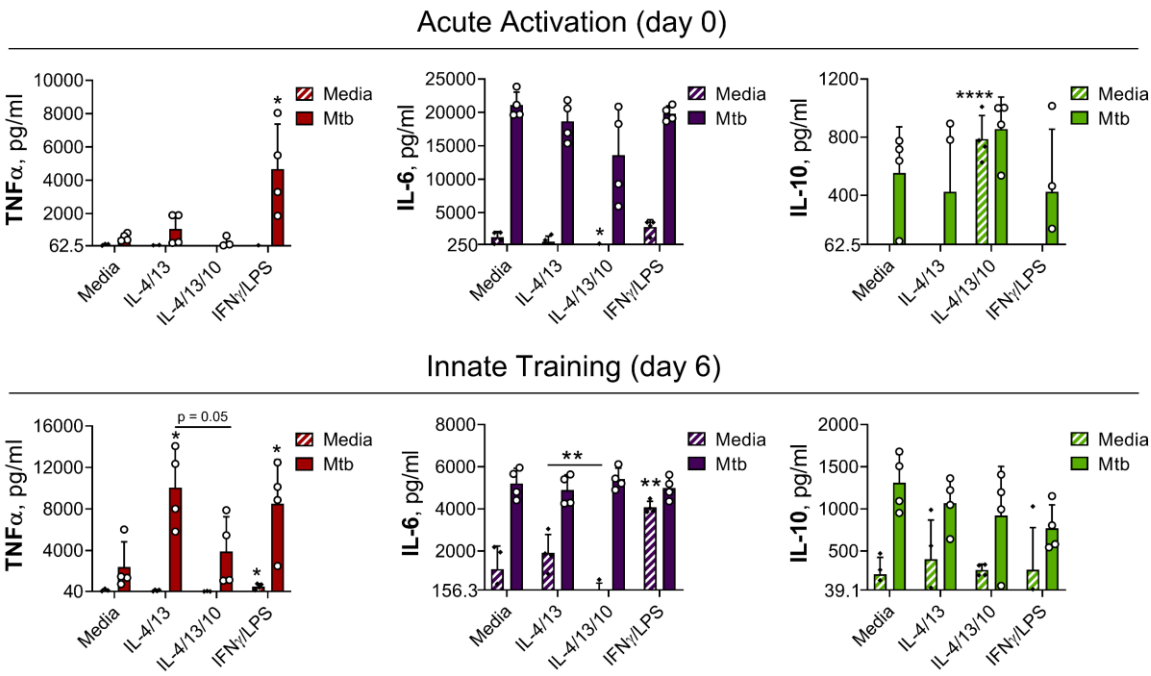

Figure 7. IL-4 and IL-13 innate training enhances MoDM secreted TNFα following Mtb stimulation
Cytokine secretion following MoDM 24 h incubation with irradiated *M. tuberculosis* (Mtb) or media on Day 0 or on Day 6 as indicated. MoDM were previously incubated with media, IL-4 with IL-13 – with or without the addition of IL-10 – or IFNγ with LPS on Day -1 for 24 h (n = 4, each rep shown by a symbol). Mean ± SD are shown and analyzed by student's t-test, compared with media control or comparing IL-4/IL-13 training with or without IL-10, as indicated. * $p \leq 0.05$, ** $p \leq 0.01$, *** $p \leq 0.001$, **** $p \leq 0.0001$.

581 In response to a secondary challenge following acute activation, on Day 0, only MoDMs activated with
582 IFNγ and LPS demonstrated enhanced TNFα secretion (**Figure 7**), whilst MoDMs activated with IL-4
583 and IL-13 demonstrated similar cytokine levels as the naïve control. At this time point, the addition of
584 IL-10 resulted in significant background secretion of IL-10 and reduced IL-6 secretion following
585 secondary stimulation with PAM3CSK4 (**Figure S8**), but otherwise cytokine levels were comparable to
586 the naïve control and MoDM activated with IL-4 and IL-13 alone. By contrast, following Mtb
587 stimulation on Day 6, MoDMs trained with either IL-4 and IL-13 or IFNγ and LPS demonstrated
588 significantly enhanced TNFα secretion compared with untrained cells, whilst secretion of IL-6 and IL-
589 10 was unaffected (**Figure 7**). This result was also apparent following secondary challenge with
590 PAM3CSK4 (**Figure S8**), although for MoDMs activated with IL-4 and IL-13, this marked increase was
591 not statistically significant. Moreover, the IL-4 and IL-13 induced enhancement of TNFα was impeded
592 by the addition of IL-10.

593 These results showed that prior activation with IL-4 and IL-13 can specifically enhance
594 inflammatory responses to subsequent challenge, and that this phenomenon is impeded by
595 concurrent IL-10 incubation. This data overall reproduced key results shown previously in the BMDM
596 training model, intimating that these findings may be applicable to human macrophages.

597

598 ## Discussion

599 Although "classical" and "alternative" activation are used to describe the two extremes of
600 macrophage polarization, the reality is a broad spectrum of activation states, affected by a multitude
601 of signals. Moreover, growing evidence has shown that the macrophage population during *M.*
602 *tuberculosis* infection is highly heterogeneous, and thus elucidating which subtypes best contain the
603 bacterium is critical for understanding disease control (A. Khan, Singh, Hunter, & Jagannath, 2019).
604 Alternative macrophage activation is moreover relevant to TB pathology, both because alveolar
605 macrophages – the initial hosts of *M. tuberculosis* upon infection – are biased towards alternative
606 activation (Huang, Nazarova, & Russell, 2019), and also considering the influence of concurrent
607 parasitic infection. Although the current study does not directly consider TB pathology, the results
608 nevertheless demonstrate that alternative macrophage activation stimuli impact innate immune
609 memory, which is an additional dimension to the noted diversity among macrophage populations.
610 Moreover, the current work demonstrates that this is, at least in part, driven via epigenetic
611 modification (**Figure S4A**), although further research is required to comprehensively map which
612 changes are occurring. The relevance of the current study, in the context of mycobacterial infection,
613 is the identification of a macrophage phenotype that is counterintuitively induced by cytokines
614 associated with suboptimal bacterial containment.

615 Whilst alternatively activated macrophages have been demonstrated to provide an
616 intracellular environment that is favorable for TB growth (Kahnert et al., 2006), resulting in greater
617 bacterial burden (Moreira-Teixeira et al., 2016) in an acute setting, there have been some conflicting
618 data concerning the interplay between parasites and mycobacterial infections. Parasitic infection has
619 been shown to enhance mycobacterial bacterial burden *in vivo* (Monin et al., 2015; Potian et al., 2011)
620 and enhance human TB pathology (Amelio et al., 2017; Mabbott, 2018), but has in some cases also
621 been shown to enhance protection against mycobacterial infection (Aira, Andersson, Singh, McKay, &
622 Blomgran, 2017; O'Shea et al., 2018). Furthermore, discrepancies have been highlighted specifically
623 regarding macrophage activation. In a model of *M. tuberculosis* macrophage infection *in vitro*, prior
624 incubation (48hr) with antigens from *Hymenolepis diminuta*, *Trichuris muris* and *Schistosoma mansoni*
625 resulted in alternative macrophage activation, but only incubation with the *H. diminuta* and *T. muris*
626 antigens resulted in enhanced mycobacterial growth (Aira et al., 2017). Moreover, the increased
627 growth was accompanied by enhanced secretion of IL-10. This however was not surprising, given that
628 IL-10 has been demonstrated to prevent phagolysosome maturation in human macrophages (O'Leary
629 et al., 2011) and promote TB disease progression in mice (Beamer et al., 2008). Herein, an additional
630 mechanism is proposed, as IL-10 appears to be a key determinant of alternative macrophage training
631 and subsequent control of mycobacterial challenge.

632 BMDM activation with IL-4 and IL-13, with or without the addition of IL-10, resulted in similar
633 activation states: comparable expression of *Arg1*, *Retnla* and *Chil3* on Day 0 (**Figure 6B**) and 7 (**Figure**
634 **S7C**), reduced expression of CD80 and upregulation of CD206 on Day 0 (**Figure S7B**), as well as reduced
635 secretion of cytokines TNFα, IL-6 and IL-10 following stimulation with Mtb on Day 0 (**Figure S7A**).
636 Whilst this hyporesponsive profile was maintained in the M(4/13/10), the trained M(4/13) on the
637 other hand demonstrate enhanced pro-inflammatory and bactericidal mechanisms in response to
638 mycobacterial challenge a week after initial activation (**Figure 6**). This intimated that IL-10 was a
639 negative regulator of innate training induced by IL-4 and IL-13 and supports that distinct cytokine
640 mediated modes of alternative macrophage activation differ regarding their innate memory
641 programming. Although a mechanism has not been identified, that IL-10 can modulate innate training
642 was herein further demonstrated by investigating innate memory induced by β-glucan (**Figure 6G**),
643 where the addition of IL-10 during the training stage resulted in attenuated cytokine secretion
644 following secondary LPS stimulation. This discovery has thereby exposed an exciting avenue for future
645 research in this field.

646 Going back to the trained M(4/13): in response to mycobacterial challenge these cells adopted
647 a phenotype similar to classically activated BMDMs: a skewing towards pro-inflammatory cytokine
648 secretion with concomitant increased expression of *Nos2* and NO production (**Figure 2**), as well as

649 enhanced mycobacterial killing capacity (**Figure 1**). Classical macrophage activation is intrinsically
650 linked with a glycolytic shift in metabolism; it is thus not surprising that prior work has identified an
651 enhancement of glycolysis as critical for efficient *M. tuberculosis* killing (Gleeson et al., 2016; Huang
652 et al., 2018) and that impeding glycolysis attenuates macrophages ability to control TB infection
653 (Hackett et al., 2020). Moreover, upon *M. tuberculosis* infection, macrophages appear to undergo a
654 biphasic metabolic profile, where they switch from an initial increase in glycolytic metabolism to an
655 enhancement of the TCA cycle and OXPHOS; a switch which allows mycobacterial survival and disease
656 progression (Shi et al., 2019). As such, it was expected that the trained M(4/13) would shift towards
657 glycolytic metabolism. However, this was not the case, as Mtb stimulation resulted in enhanced OCR
658 and SRC, indicating the use and upregulation of OXPHOS (**Figure 3**). Furthermore, LC-MS analysis of
659 metabolites indicated increased use of FAO, as well as enhanced creatine, further supporting the
660 continued use of M2-typical metabolism. This was moreover confirmed with the use of the ATP
661 synthase inhibitor oligomycin, where it was demonstrated that inhibition of OXPHOS reduced trained
662 M(4/13) cytokine secretion, whereas by contrast M(IFNγ/LPS) TNFα upregulation was unaffected.
663 Furthermore, when trained M(4/13) were incubated in a glucose depleted environment during the
664 week preceding secondary stimulation, the glucose depletion enhanced the pro-inflammatory shift:
665 increased TNFα and IL-6 secretion combined with reduced IL-10 production (**Figure 4B**). This was a
666 stark contrast to the effect of glucose depletion on untrained M(-) and trained M(IFNγ/LPS), where
667 the secretion of all measured cytokines was attenuated. This contrast between M(4/13) and
668 M(IFNγ/LPS) cemented their differences regarding metabolic dependency on glucose. It should be
669 noted that prior work has identified differences in macrophage metabolic profiles in response to
670 infection with live *M. tuberculosis* compared with the killed bacterium or infection with attenuated
671 BCG (Cumming, Addicott, Adamson, & Steyn, 2018). However, the consensus is that classic
672 macrophage activation, and an accompanying shift to glycolytic metabolism, is paramount for
673 effective mycobacterial killing and propagation of inflammatory responses. It is surprising therefore
674 that these results summarily intimated that trained M(4/13) do not rely on glycolysis to fuel anti-
675 mycobacterial responses.

676 It is of note moreover that the addition of a glycolysis inhibitor reduced cytokine secretion,
677 from M(-), M(IFNγ/LPS), as well as M(4/13) following secondary stimulation (**Figures S6A-B**). That
678 inhibition of glycolysis impeded pro-inflammatory cytokine secretion, but glucose depletion did not,
679 indicated that glycolysis in trained M(4/13) was fueling the TCA cycle and downstream OXPHOS, and
680 upon glucose depletion other pathways, such as glutaminolysis, were compensating for this loss.
681 Glutaminolysis has been shown to be upregulated following macrophage activation with IL-4 and has
682 been demonstrated to compensate for glycolysis inhibition in driving the TCA cycle and OXPHOS

683 (Wang et al., 2018). In the present study, it was moreover observed that the use of a glutaminolysis
684 inhibitor reduced TNFα and IL-6 secretion following secondary stimulation in trained M(4/13)
685 specifically, and not in untrained M(-) or M(IFNγ/LPS) (**Figure 4A**). This work suggests that OXPHOS
686 can be important for pro-inflammatory responses, an observation that is supported by previous work
687 demonstrating that for instance mitochondrial stress is a mechanism of macrophage tolerance
688 (Timblin et al., 2021) and that the ETC is important for nod-like receptor family pyrin domain
689 containing 3 (NLRP3) inflammasome activity (Billingham et al., 2022). It should be noted that in the
690 latter study however, LPS induced TNFα secretion was not impeded by inhibition of ETC complexes I
691 and II, demonstrating once more that the metabolic phenotype of the trained M(4/13), explored in
692 the current study, is highly unexpected and warrants further study.

693 The metabolic profile in trained M(4/13), as summarized in **Figure 5**, is not only distinct from
694 classically activated macrophages, but also from that seen with other training stimuli, such as β-glucan.
695 Innate training is being tested as a means to bolster innate immunity against *M. tuberculosis* (Khader
696 et al., 2019) and it was recently reported that training with β-glucan was protective against subsequent
697 *M tuberculosis* infection, as seen by enhanced human monocyte pro-inflammatory cytokine secretion
698 and increased mouse survival *in vivo* (Moorlag et al., 2020). Similar to classical macrophage activation,
699 β-glucan training results in a glycolytic shift, as demonstrated in human monocytes (Cheng et al.,
700 2014). As such, the phenotype of the trained M(4/13) is distinct from other macrophage phenotypes
701 previously demonstrated to protect against TB, and thus offers an additional avenue for future
702 research regarding strategies for combatting this disease.

703 It should be noted moreover, that these experiments have been carried out in a murine *in*
704 *vitro* system and how translational these findings are, not only to TB *in vivo* infection models, but also
705 how relevant this is in a human context remains to be elucidated. Preliminary work herein has
706 demonstrated that human monocyte derived macrophages trained with IL-4 and IL-13 show a
707 markedly enhanced secretion of TNFα in response to secondary stimulation with either irradiated Mtb
708 (**Figure 7**) or PAM3CSK4 (**Figure S8**). Moreover, this enhancement was impeded by the addition of IL-
709 10 during the training stage, showing very similar macrophage phenotypes as the BMDM model. This
710 promising result intimates that these findings may well be relevant in a human context, although
711 further research is required to further examine this macrophage phenotype and explore its potential
712 role in TB infection.

713 Van den Bossche et al. in 2016 highlighted a key adaptive distinction between classical and
714 alternative macrophage activation: that alternatively activated macrophages can be "re-polarized"
715 due to their metabolic versatility, whereas the mitochondrial dysfunction which occurs during classical
716 macrophage activation prevents such reprogramming (Van den Bossche et al., 2016). In the current

study, an additional adaptive capacity is identified: that activation with IL-4 and IL-13 programs BMDMs to better respond to a mycobacterial challenge, whilst crucially retaining their metabolic diversity.

In conclusion, our work presents mechanistic insight into how innate training via IL-4 and IL-13 can enhance macrophage pro-inflammatory responses and mycobacterial killing. This unexpected finding shows how macrophage plasticity belies the usual M1-M2 dichotomy and provides a new framework to explore the impact of comorbidities, such as parasitic infections, on TB disease burden.

Materials and Methods

Table 1. Sources of materials and resources

REAGENT or RESOURCE	SOURCE	IDENTIFIER
Antibodies		
Anti-CD11b-APC-eFluor 780	Thermo Fisher Scientific, Waltham, Massachusetts	Cat# 47-0112-82, RRID: AB_1603193, Clone M1/70
Anti-CD206-PE	BioLegend, San Diego, California	Cat# 141706, RRID: AB_10895754, Clone C068C2
Anti-CD80-FITC	BD Biosciences, Franklin Lakes, New Jersey	Cat# 561954, RRID: AB_10896321, Clone 16-10A1
Anti-F4/80-PerCP-Cy5.5	Thermo Fisher Scientific, Waltham, Massachusetts	Cat# 45-4801-82, RRID: AB_914345, Clone BM8
Anti-Histone H3 (rabbit)	Active Motif, Carlsbad, Canada	Cat# 39763
Anti-H3K4me3	Abcam, Boston, Massachusetts	Cat# ab8580
Anti- H3K9me2	Abcam, Boston, Massachusetts	Cat# ab1220
Anti-H3K27me3	Active Motif, Carlsbad, Canada	Cat# 61017
Anti-MHC class II-eFlour 450	Thermo Fisher Scientific, Waltham, Massachusetts	Cat# 48-5321-82, RRID: AB_1272204, Clone M5/114.15.2
Anti-mouse IgG	LI-COR, Lincoln, Nebraska	Cat# 925-32210
Anti-Rabbit IgG	LI-COR, Lincoln, Nebraska	Cat# 926-32211

Fc block: Anti-CD16/CD32	BD Biosciences, Franklin Lakes, New Jersey	Cat# 553142, RRID: AB_394657, Clone 2.4G2
Bacterial and virus strains		
Non-viable irradiated *Mycobacterium tuberculosis* strain H37Rv	BEI resources, Manassas, Virginia	NR-49098
Bacille Calmette-Guérin (BCG) Denmark 1331	Gift to Prof. Gordon from Prof. Behr, McGill University, Canada	N/A
Chemicals, peptides, and recombinant proteins		
2-deoxyglucose, 2-DG	Sigma Aldrich, Burlington, Massachusetts	Cat# D8375
4% PFA in PBS	Santa Cruz Biotechnology, Dallas, Texas	Cat# NC0238527
Acetonitrile	Thermo Fisher Scientific, Waltham, Massachusetts	Cat# 10001334
Antimycin-A	Sigma Aldrich, Burlington, Massachusetts	Cat# A8674
BPTES	Sigma Aldrich, Burlington, Massachusetts	Cat# SML0601-5mg
CpG	InvivoGen, San Diego, California	Cat# ODN M362
DMEM (high glucose)	Sigma Aldrich, Burlington, Massachusetts	Cat# D5671
DMEM (no glucose)	Gibco, Waltham, Massachusetts	Cat# 11966025
dNTP Mix	Meridian Bioscience, Cincinnati, Ohio	Cat# BIO-39028
FBS	Biosera, Kansas City, Missouri	Batch# 015BS551
FCCP	Sigma Aldrich, Burlington, Massachusetts	Cat# C2920
Fixable Viability Stain 510	Invitrogen, Waltham, Massachusetts	Cat# 564406

Glucose	Sigma Aldrich, Burlington, Massachusetts	Cat# G8270
L-Glutamine	Gibco, Waltham, Massachusetts	Cat# 25030-024
Glycerol	Sigma Aldrich, Burlington, Massachusetts	Cat# G2025
Heat-Shocked Bovine Serum Albumin (BSA)	Thermo Fisher Scientific, Waltham, Massachusetts	Cat# 12881630
Hoechst 33342	Thermo Fisher Scientific, Waltham, Massachusetts	Cat# 10150888
KAPA SYBR® FAST Rox low qPCR Kit Master Mix	Sigma Aldrich, Burlington, Massachusetts	Cat# KK4622
LPS, *Escherichia coli*, serotype R515	Enzo, Farmingdale, New York	Cat# ALX-581-007-L002
Lymphoprep™	Stemcell Technologies, Vancouver, Canada	Cat# 07851
Methanol	Thermo Fisher Scientific, Waltham, Massachusetts	Cat# 10284580
Middlebrook 7H11 powder	Sigma Aldrich, Burlington, Massachusetts	Cat# M0428
Middlebrook 7H9 powder	Sigma Aldrich, Burlington, Massachusetts	Cat# M0178
M-MLV reverse transcriptase	Promega, Madison, Wisconsin	Cat# M3683
Modified Auramine-O stain and quencher	Scientific Device Laboratory, Des Plaines, Illinois	Cat# 345-04L
MTA	Sigma Aldrich, Burlington, Massachusetts	Cat# D5011-25MG
Oligomycin	Sigma Aldrich, Burlington, Massachusetts	Cat# 75351
PAM3CSK4	InvivoGen, San Diego, California	Cat# tlrl-pms

PBS, sterile	Gibco, Waltham, Massachusetts	Cat# 14190094
Penicillin-Streptomycin	Gibco, Waltham, Massachusetts	Cat# 15-070-063
Phalloidin-Alexa Fluor 647	Invitrogen, Waltham, Massachusetts	Cat# A22287
Poly I:C	InvivoGen, San Diego, California	Cat# tlrl-pic
Pyruvate	Sigma Aldrich, Burlington, Massachusetts	Cat# P5280
Radio-Immunoprecipitation Assay (RIPA) buffer	Sigma Aldrich, Burlington, Massachusetts	Cat# R0278-50ML
Random Hexamer Primer Mix	Meridian Bioscience, Cincinnati, Ohio	Cat# BIO-38028
Recombinant human IFNγ	Peprotech, Cranbury, New Jersey	Cat# 300-02
Recombinant human IL-10	Peprotech, Cranbury, New Jersey	Cat# 200-10
Recombinant human IL-13	Peprotech, Cranbury, New Jersey	Cat# 200-13
Recombinant human IL-4	Peprotech, Cranbury, New Jersey	Cat# 200-04
Recombinant human M-CSF	Prospec Protein Specialists, Rehovot, Israel	Cat# CYT-308
Recombinant murine IFNγ	Peprotech, Cranbury, New Jersey	Cat# 315-05
Recombinant murine IL-10	Peprotech, Cranbury, New Jersey	Cat# 210-10
Recombinant murine IL-13	Peprotech, Cranbury, New Jersey	Cat# 210-13
Recombinant murine IL-4	Peprotech, Cranbury, New Jersey	Cat# 214-14
Resiquimod/R848	InvivoGen, San Diego, California	Cat# tlrl-r848
Reverse Transcriptase Buffer	Promega, Madison, Wisconsin	Cat# A3561
RNAseOUT	Invitrogen, Waltham, Massachusetts	Cat# 10777019
Rotenone	Sigma Aldrich, Burlington, Massachusetts	Cat# R8875

RPMI 1640 Glutamax	Gibco, Waltham, Massachusetts	Cat# 21875034
Seahorse Calibration Fluid pH 7.4	Agilent, Santa Clara, California	Part# 100840-000
Seahorse XF DMEM Medium	Agilent, Santa Clara, California	Cat# 103575-100
Sodium Chloride	Sigma Aldrich, Burlington, Massachusetts	Cat# S9888
Tween20	Sigma Aldrich, Burlington, Massachusetts	Cat# P1379-1L
Valine-d8	CK isotopes, Newtown Unthank, UK	Cat# DLM-488
Vectashield mounting media	VWR, Vector Laboratories	Cat# 101098-042
Water, sterile	Baxter, Deerfield, Illinois	Cat# UKF7114
WGP Dispersible	InvivoGen, San Diego, California	Cat# tlrl-wgp
Critical commercial assays		
BCA Protein Assay Kit (Pierce™)	Thermo Fisher Scientific, Waltham, Massachusetts	Cat# 23225
Griess Reagent System kit	Promega, Madison, Wisconsin	Cat# G2930
High Pure RNA Isolation Kit	Roche, Basel, Switzerland	Cat# 11828665001
Human IL-10 ELISA Kit uncoated	Invitrogen, Waltham, Massachusetts	Cat# 88710688
Human IL-6 ELISA Kit uncoated	Invitrogen, Waltham, Massachusetts	Cat# 88706688
Human TNFα ELISA Kit uncoated	Invitrogen, Waltham, Massachusetts	Cat# 88734688
Mouse IL-10 ELISA MAX	BioLegend, San Diego, California	Cat# 431411
Mouse IL-6 ELISA MAX	BioLegend, San Diego, California	Cat# 431301
Mouse TNFα DuoSet ELISA	R&D Systems, Minneapolis, Minnesota	Cat# DY410
Deposited data		

Raw and analyzed data	This Paper	DOI: 10.17632/ncbph43m85.1.
Experimental models: Cell lines		
L929	gift of Prof. Muñoz-Wolf, Trinity College, Dublin	N/A
L929	gift of Prof. Sheedy, Trinity College, Dublin	N/A
Experimental models: Organisms/strains		
WT mice used for cell isolations	In-house colonies	C57BL/6JOlaHsd
Oligonucleotides		
Primers for *Actb*	See Table S1	N/A
Primers for *Arg1*	See Table S1	N/A
Primers for *Chitl3*	See Table S1	N/A
Primers for *Ldha*	See Table S1	N/A
Primers for *Myc*	See Table S1	N/A
Primers for *Nos2*	See Table S1	N/A
Primers for *Pkm2*	See Table S1	N/A
Primers for *Retnla*	See Table S1	N/A
Primers for *Sdha*	See Table S1	N/A
Primers for *Tbp*	See Table S1	N/A
Software and algorithms		
FlowJo 7	FlowJo LLC, Franklin Lakes, New Jersey	https://www.flowjo.com/solutions/flowjo
ImageJ	National Institutes of Health and the Laboratory for Optical and Computational Instrumentation	https://imagej.nih.gov/ij/
MetaboAnalyst 5.0	Xia Lab @ McGill	https://www.metaboanalyst.ca/
Microsoft Office Excel	Microsoft, Redmond, Washington	https://products.office.com/en-au/excel
Prism 8.2	GraphPad Software, San Diego, California	https://www.graphpad.com/scientific-software/prism/

Tracefinder 5.0	Thermo Fisher Scientific, Waltham, Massachusetts	https://www.thermofisher.com/ie/en/home/industrial/mass-spectrometry/liquid-chromatography-mass-spectrometry-lc-ms/lc-ms-software/lc-ms-data-acquisition-software/tracefinder-software.html

Experimental Model and Subject Details

Animals

Mice used for primary cell isolation were eight to 16-week-old wild-type C57BL/6 mice that were bred in the Trinity Biomedical Sciences Institute Bioresources Unit. Animals were maintained according to the regulations of the Health Products Regulatory Authority (HPRA). Animal studies were approved by the TCD Animal Research Ethics Committee (Ethical Approval Number 091210) and were performed under the appropriate license (AE191364/P079).

Cell Isolation and Culture

Bone marrow-derived macrophages (BMDMs) were generated as described previously by our group (Lebre, Hanlon, Boland, Coleman, & Lavelle, 2018). Briefly, bone marrow cells were extracted from the leg bones and were cultured in high glucose DMEM, supplemented with 8% v/v fetal bovine serum (FBS), 2 mM L-glutamine, 50 U ml^{-1} penicillin, 50 µg ml^{-1} streptomycin (hereafter referred to as complete DMEM [cDMEM]). Cells were plated on non-tissue cultured treated petri dishes (Corning) on day -8. Fresh medium was added on day -5 and on day -2 adherent cells were detached by trypsinization and collected. Unless specified otherwise, for acute/polarization studies, BMDMs were seeded in 12-well plates at 0.9×10^6 BMDMs per well, and for training studies, BMDMs were seeded in 24-well plates at 0.2×10^6 BMDMs per well.

On day -1 BMDMs were cultured with medium (naïve/untrained) or activated with 25 ng ml^{-1} IFNγ, 10 ng ml^{-1} LPS, 40 ng ml^{-1} IL-4, 20 ng ml^{-1} IL-13, 40 ng ml^{-1} IL-10, 100 µg ml^{-1} whole β-glucan particles (WGP Dispersible) – derived from the yeast *Saccharomyces cerevisiae* – or a combination of one or more activation stimuli, as specified in relevant figure legends. After 24 hours, the supernatant was replaced with fresh media. For acute activation/polarization studies, the BMDMs were left to rest for 2 hours before experiment. For training studies, the BMDMs were left to rest, fed on day 3 or 4

752 and experiments were carried out on day 6. The cDMEM used was supplemented with L929 cell line
753 conditioned media, containing macrophage colony-stimulating factor (M-CSF) where two different
754 batches were used. For all experimental repeats where β-glucan was used with or without the addition
755 of IL-10, 20-, 20- 10-, 7- and 5% were used on days -8, -5, -2, 0 and 3/4 respectively (L929 batch gifted
756 by Prof. Sheedy). For all other experiments 25-, 25-, 15-, 10- and 7% were used on days -8, -5, -2, 0
757 and 3/4 respectively (batch gifted by Prof. Muñoz-Wolf).

758 To generate human monocyte-derived macrophages (MoDMs), mononuclear cells were isolated on
759 day -7 from peripheral blood buffy coats obtained from the Irish Blood Transfusion Services (Dublin,
760 Ireland) using density gradient centrifugation with Lymphoprep. Cells were cultured on plastic in RPMI
761 media supplemented with 10% FBS (hereafter referred to as complete RPMI [cRPMI]) and 20 ng ml^{-1}
762 recombinant human M-CSF at 1×10^6 cells ml^{-1}, seeded at 2×10^6 cells per well. On day -4, 1 ml of
763 media was carefully removed from each well and replaced with fresh cRPMI, supplemented with 20
764 ng ml^{-1} recombinant human M-CSF. Non-adherent cells were removed by washing once on day -1 with
765 pre-warmed PBS and incubated with cRPMI, supplemented with 5 ng ml^{-1} M-CSF. After a minimum of
766 4 hours of rest, either more media was added (naïve/untrained) or the MoDMs were activated with
767 20 ng ml^{-1} recombinant human IFNγ with 5 ng ml^{-1} LPS or 20 ng ml^{-1} IL-4 with 10 ng ml^{-1} IL-13, the latter
768 with or without 20 ng ml^{-1} IL-10. After 24 hours (day 0), the media was removed and replaced with
769 cRPMI, supplemented with 5 ng ml^{-1} M-CSF. For acute activation/polarization studies, the MoDMs
770 were left to rest for 2 hours before experiment. For training studies, the MoDMs were left to rest, fed
771 on day 3 (media supplemented with 2.5 ng ml^{-1} M-CSF) and experiments were carried out on day 6.
772 Supply of human blood products from IBTS was approved by clinical indemnity to F. Sheedy.

773 **BCG Infection**

774 Mature BMDMs were seeded in 24-well plates at 0.5×10^6 cells (acute activation) or 0.2×10^6 cells
775 (training) per well on day -2. For imaging of internalized BCG in untrained and trained BMDMs, $0.2 \times$
776 10^6 BMDMs were seeded on circular glass coverslips (placed in 24 well plates, one coverslip per well)
777 that had been previously treated with sodium hydroxide to aid attachment.

778 BMDMs were incubated with media (naïve) or activated as outlined above on day -1, for 24
779 hours before BMDMs were washed and fresh media was added. For acute activation studies, BMDMs
780 were infected with BCG Denmark minimum 3 hours later. For training studies, BMDMs were fed on
781 day 3 and infected with BCG Denmark on Day 6. At the time of infection, the media was removed and
782 replaced with fresh media, either with or without (negative control) bacteria.

783 Regarding infection dose (BCG per cell), for infection in acutely activated BMDMs, cell number
784 per well was assumed to be 0.5×10^6. For infecting trained BMDMs, three extra wells were prepared
785 for all conditions and BMDMs were removed from these wells by trypsinization on day 5, pooled and

786 counted in triplicate. Prepared BCG single cell suspension (see below) was diluted to reach an intended
787 infection dose of 5 BCG per cell (as measured by OD_{600}, where 0.1 is estimated to be 10×10^6 bacteria
788 ml^{-1}). Each infection dose was measured via CFU counts (see below) and was thus subsequently
789 corrected to an actual infection dose of roughly 30 BCG per cell.
790 3 hours post infection the supernatant was removed and the infected BMDMs were washed
791 twice with Dulbecco's Phosphate Buffered Saline (PBS) to remove extracellular bacteria, and fresh
792 media was added.
793 To measure cytokine secretion at each time point (3-, 27- and 51 hours post infection),
794 supernatant was collected and filtered (polyethersulfone [PES] 0.22 µm Luer lock syringe filter; Millex-
795 GP) to remove BCG, prior to specific cytokines being measured by ELISA.
796 For CFU counts, at each time point the media was removed, wells were washed once with PBS
797 before the BMDMs were lysed with 0.05% Tween20 in water. The cell lysate was diluted in pre-
798 warmed (37 °C) 7H9 media, and 50 µl of dilutions 10^{-2}-10^{-6} were spread onto enriched 7H11 agar plates
799 by dotting. Agar plates were incubated at 37 °C for 6 weeks and colonies were counted once a week
800 from week 2 and on. CFU counts 3 hours gave the multiplicity of infection (MOI). Killing was assessed
801 by the difference in CFU counts following the 3-hour time point, see accompanying dataset for
802 comprehensive calculations.
803 For imaging internalized BCG (wells containing glass coverslips), media was removed, BMDMs
804 were washed with PBS and then fixed with 4% paraformaldehyde (in PBS) overnight. The
805 paraformaldehyde was then removed and coverslips were stored in PBS.
806
807 **Stimulation Experiments**
808 Naïve (media control) or activated BMDMs were incubated with media or secondary stimuli on day 0
809 (acute activation/polarization) or day 6 (training). Secondary stimuli: 150 µg ml^{-1} gamma-irradiated
810 whole cells of *Mycobacterium tuberculosis* strain H37Rv (concentration measured by OD_{600}, where 100
811 mg ml^{-1} was 0.32), 35 ng ml^{-1} PAM3CSK4, 25 ng ml^{-1} LPS, 5 µg ml^{-1} Poly I:C, 0.55 µg ml^{-1} R848, 10 µg ml^{-}
812 ^{1} CpG.
813 For histone methylation inhibition: on day -2 BMDMs were incubated with MTA (final
814 concentration 1 mM) one hour prior to media incubation or activation as outlined above.
815 For metabolic inhibition experiments: on day 6 BMDMs were pre-incubated with 1mM 2-DG
816 for 3 hours, 2 µM oligomycin or 10 µM BPTES 1 hour prior to media incubation or secondary
817 stimulation.
818 For glucose depletion training experiment: untrained or trained BMDMs were incubated with
819 either the regular high glucose cDMEM or glucose depleted cDMEM, with DMEM devoid of glucose

820 (Gibco), from day -2 until incubation with media or secondary stimulation on Day 6 (fed day 3 with the
821 same media as given on day -2). Note, the glucose depleted cDMEM included 8% v/v FBS and the same
822 amount of L929 conditioned media as outlined previously, both of which provided a source of glucose.

823 Naïve (media control) or activated MoDMs were incubated with media or secondary stimuli on day 0
824 (acute activation/polarization) or day 6 (training). Secondary stimuli: 250 µg ml^{-1} gamma-irradiated
825 whole cells of *Mycobacterium tuberculosis* strain H37Rv, 100 ng ml^{-1} PAM3CSK4.

826 **Seahorse**

827 All real-time measurements of oxygen consumption rate (OCR) and extracellular acidification rate
828 (ECAR) were measured by using Seahorse system: Seahorse XFe96 Analyzer (Agilent). The analysis
829 used was a Mitochondrial Stress Test (using a standard Agilent Seahorse protocol).

830 On day -2, mature BMDMs were seeded in a 96-well Seahorse plate (Agilent): 100,000 cells
831 per well for acute activation studies or 30,000 cells per well for training studies. BMDMs were
832 activated on day -1 as outlined and analyzed on either day 0 (24 hours after activation) or day 6 (fed
833 on day 3), with or without secondary stimulation on day 5 (training studies).

834 The day before analysis, a Seahorse Cartridge (Agilent) was incubated overnight at 37 °C
835 (incubator devoid of CO_2). The following day, the sterile water was replaced with Calibration Fluid at
836 pH 7.4 incubated as before for 90 minutes before the analysis.

837 An hour before the analysis, in the Seahorse plate regular cDMEM was replaced with Seahorse
838 XF DMEM, supplemented with 10 mM glucose, 1 mM pyruvate and 2 mM L-glutamine. The BMDMs
839 were then incubated for an hour at 37 °C (incubator devoid of CO_2).

840 15 minutes before the analysis, the cartridge was removed and reagents/inhibitors were
841 added to their respective ports: oligomycin (port A, final concentration 10 µM), FCCP (port B, final
842 concentration 10 µM), rotenone and antimycin-A (port C, final concentrations 5 µM each).

843 The analysis was carried out according to the manufacturer's instructions. Recorded values
844 less than zero were disregarded.

845 For training experiments, protein concentration was used to standardize the OCR and ECAR
846 measurements. Supernatant was removed, cells were washed once in PBS and 10 µl of RIPA buffer
847 was added per well. After pipetting up and down and scraping, the buffer was collected and samples
848 from the same condition were pooled. 20 µl of pooled solution was used to measure protein
849 concentration, using the Pierce bicinchoninic acid (BCA) assay kit (Thermo Scientific) according to the
850 manufacturer's instructions (microplate procedure). Absorbance was measured at 560 nm.
851

Metabolomics (LC-MS) sample preparation

On day -2, BMDMs were seeded in 6-well plates: 1×10^6 cells per well and activated on day -1 with IL-4/13 as outlined or incubated with media. BMDMs were fed on day 3 and incubated with irradiated *M. tuberculosis* on Day 6 for 24 hours. Prior to metabolite extraction, cells were counted using a separate counting plate prepared in parallel and treated exactly like the experimental plate. Supernatant was removed and cells were washed once in PBS. After aspiration, the BMDMs were kept at -80 °C or on dry ice. Metabolites were extracted by adding chilled extraction buffer (500 µl/1×10^6 cells), followed by scraping (carried out on dry ice). Buffer was transferred to chilled eppendorf tubes and shaken in a thermomixer at maximum speed (2000 rpm) for 15 minutes at 4 °C. Following centrifugation at maximum speed for 20 minutes, roughly 80% of supernatant was transferred into labelled LC-MS vials, taking care to avoid pellet and any solid debris.

Western blot sample preparation

On day -2, BMDMs were seeded in 6-well plates: 1×10^6 cells per well and activated on day -1 with IL-4/13 or β-glucan as outlined, or incubated with media as an untrained control. BMDMs were fed on day 3 and on day 6, the cells were washed once with PBS, before being lysed with RIPA buffer.

Flow Cytometry

On day -2, 0.8×10^6 mature BMDMs were seeded on non-tissue cultured treated 35 mm petri dishes (Corning) and activated as previously outlined on Day -1. The naïve or activated/trained BMDMs were harvested at two separate time points: day 0 (24 hours post activation for acute activation characterisation) or day 6 (fed on day 3), with or without secondary stimulation on day 5 as specified in figure legends (training experiments).

For analysis, BMDMs were placed on ice for 30 min before harvesting with PBS-EDTA (5 mM) solution by gently pipetting up and down and transferring to flow cytometry tubes. Cells were incubated with Fixable Viability Stain 510 at RT for 15 min. After washing with PBS, cells were stained with anti-mouse Fc block, 15 minutes prior staining with CD80-FITC, CD206-PE, F4/80-PerCP-Cy5.5, CD11b-APC-eFluor 780, MHC class II-eFluor 450 for an additional 30 min at 4 °C. The cells were washed with PBS and resuspended in flow cytometry buffer (1% FBS in PBS). Samples were acquired on a BD Canto II flow cytometer and the data was analysed by using FlowJo software.

Method Details

BCG Preparation and Plating

Bacille Calmette-Guérin (BCG) Denmark (OD_{600} 0.1) was incubated in 7H9 media at 37 °C with rotation until the OD_{600} 0.5-0.8 (logarithmic growth phase) was reached.

885 Single cell suspension was prepared as follows: bacteria were pelleted by centrifugation and
886 7H9 media was removed. Bacteria were vortexed with glass beads before pre-warmed (37 °C) DMEM
887 was added and bacteria were left to sediment for 5 minutes. Bacterial suspension was carefully
888 collected (avoiding disruption of the pellet) and centrifuged again to pellet large clumps. Suspension
889 was collected (avoiding the pellet). Suspension was passed through a 26G needle 15 times to
890 disaggregate bacterial clumps.
891 Bacterial concentration was estimated by OD_{600} (where 0.1 was estimated as 10×10^6 bacteria
892 ml^{-1}) and infection dose was confirmed by colony forming unit (CFU) counts.
893 7H11 agar plates (for CFU counts) were made up as follows: 10.5 g middlebrook 7H11 powder
894 and 2.5 ml glycerol was dissolved in distilled water to reach 500 ml and autoclaved. Once cooled
895 sufficiently, 50 ml sterile-filtered (0.22 µm; SteriCup [Millipore]) albumin-dextrose-sodium chloride
896 (ADN) enrichment was added. For 1 liter of ADN enrichment: 50 g fatty acid-free, heat-shocked bovine
897 serum albumin, 8.5 g sodium chloride and 20 g glucose were dissolved in sterile water to reach 1 liter.
898
899 **Staining and Imaging of Internalized BCG**
900 For staining the coverslips contained in 24-well plates, PBS was removed and 17 µM Hoechst 33342
901 and 7.5 U Phalloidin-Alexa Fluor 647 (in 1 ml PBS) was added to each well. After half an hour (in the
902 dark), the solution was removed and the coverslips were washed with PBS. 200 µl Modified Auramine-
903 O stain was added for 2 minutes (in the dark), after which the stain was removed and the wells were
904 washed with PBS. To quench any extracellular BCG, 200 µl Auramine-O Quencher de-colorizer was
905 added for 2 minutes (in the dark) and then the quencher was removed and the coverslips were washed
906 with PBS. The coverslips were then fixed onto glass slides: 2 µl Vectashield mounting media was used
907 per coverslip and clear nail polish was applied around the edge and allowed to dry completely. The
908 coverslips were stained and imaged the same day.
909 Images of all samples were obtained using a Leica SP8 confocal microscope, taken with x40
910 magnification oil objective. Z-stack images through the entire cell were obtained and representative
911 images were taken from these stacks.

912 **Liquid Chromatography coupled to Mass Spectrometry (LC-MS)**
913 Extraction buffer for isolating metabolites: 50% LC-MS grade methanol, 30% LC-MS grade acetonitrile,
914 20% ultrapure water (internal filtration system), valine-d8 final concentration 5 µM.
915 Hydrophilic interaction chromatographic (HILIC) separation of metabolites was achieved using
916 a Millipore Sequant ZIC-pHILIC analytical column (5 µm, 2.1 × 150 mm) equipped with a 2.1 × 20 mm
917 guard column (both 5 mm particle size) with a binary solvent system. Solvent A was 20 mM ammonium
918 carbonate, 0.05% ammonium hydroxide; Solvent B was acetonitrile. The column oven and

919 autosampler tray were held at 40 °C and 4 °C, respectively. The chromatographic gradient was run at
920 a flow rate of 0.200 mL/min as follows: 0–2 min: 80% B; 2-17 min: linear gradient from 80% B to 20%
921 B; 17-17.1 min: linear gradient from 20% B to 80% B; 17.1-22.5 min: hold at 80% B. Samples were
922 randomized and analysed with LC–MS in a blinded manner with an injection volume was 5 µl. Pooled
923 samples were generated from an equal mixture of all individual samples and analysed interspersed at
924 regular intervals within sample sequence as a quality control.

925 Metabolites were measured with a Thermo Scientific Q Exactive Hybrid Quadrupole-Orbitrap
926 Mass spectrometer (HRMS) coupled to a Dionex Ultimate 3000 UHPLC. The mass spectrometer was
927 operated in full-scan, polarity-switching mode, with the spray voltage set to +4.5 kV/-3.5 kV, the
928 heated capillary held at 320 °C, and the auxiliary gas heater held at 280 °C. The sheath gas flow was
929 set to 25 units, the auxiliary gas flow was set to 15 units, and the sweep gas flow was set to 0 unit.
930 HRMS data acquisition was performed in a range of *m/z* = 70–900, with the resolution set at 70,000,
931 the AGC target at 1×10^6, and the maximum injection time (Max IT) at 120 ms. Metabolite identities
932 were confirmed using two parameters: (1) precursor ion m/z was matched within 5 ppm of theoretical
933 mass predicted by the chemical formula; (2) the retention time of metabolites was within 5% of the
934 retention time of a purified standard run with the same chromatographic method. Chromatogram
935 review and peak area integration were performed using the Thermo Fisher software Tracefinder 5.0
936 and the peak area for each detected metabolite was normalized against the total ion count (TIC) of
937 that sample to correct any variations introduced from sample handling through instrument analysis.
938 The normalized areas were used as variables for further statistical data analysis.

939 **Preparation of β-glucan Stock**

940 The β-glucan particles (WGP Dispersible) were weighed and dissolved in sterile water to yield 10-15
941 ml of 25 mg ml^{-1}. This solution was left at room temperature overnight (8-16 hours) before sonication
942 with a 150VT ultra sonic homogenizer with a 5/32" microtip. Whilst on ice, the solution was sonicated
943 for 5 minutes, at 50% power and 50% time pulse rate, while the tip was immersed roughly 5 mm below
944 the surface of the liquid. The β-glucan particles were then pelleted by centrifugation (1,000 G, 10
945 minutes, room temperature) and the water was removed by careful decanting and replaced with 0.2
946 M NaOH in water, at a volume to reach 25 mg ml^{-1}. After 20 minutes, the β-glucan was washed three
947 times with sterile water, using the same pelleting, decanting and replacement of solvent conditions
948 as described. Finally, two last washes were carried out to replace the sterile water with sterile PBS.
949 Prior to each use, the stock was thoroughly vortexed.

950 **ELISA**

951 For detection of secreted TNFα, IL-6 and IL-10 from BMDMs, supernatants were collected and
952 cytokines quantified by ELISA according to manufacturers' instructions (R&D Systems, Biolegend of
953 Invitrogen), except antibody and sample volumes were halved.

954 **Western Blot**

955 BMDMs were lysed with RIPA buffer and the whole-cell protein lysates were separated on pre-cast
956 Bolt 12% Bis-Tris Plus gels (Invitrogen, NW00127BOX) and transferred to nitrocellulose membranes.
957 Membranes were subsequently probed using the relevant primary (histone H3, H3K4me3, H3K27me3
958 and H3K9me2) and secondary antibodies (anti-IgG) and imaged using the Odyssey Fc Imager (Li-Cor).
959 Images of blots were analysed with ImageJ to calculate the relative optical density (ROD =
960 area/percentage). ROD was then standardized to the untrained/media control samples: adjusted ROD
961 values.

962 **Nitric oxide (NO) secretion**

963 NO concentrations were quantified by indirect measurement of nitrite (NO_2^-) via the Griess Reagent
964 System kit (Promega). The assay was carried out as per manufacturer's instructions and absorbance
965 of 560 nm was measured.

966 **Reverse Transcription Quantitative PCR (rt-qPCR)**

967 RNA was isolated via High Pure RNA Isolation Kit (Roche) according to the manufacturer's instructions
968 and RNA was eluted in 50 µl water. RNA (minimum 100 ng) was reverse transcribed into
969 complementary DNA (cDNA) with an M-MLV reverse transcriptase, RNase H minus, point mutant, in
970 reverse transcriptase buffer, mixed with dNTPs, random hexamer primers and ribonuclease inhibitor
971 (RNAseOUT). Quantitative PCR was performed using KAPA SYBR® FAST Rox low qPCR Kit Master Mix
972 in accordance with the instructions provided by the manufacturer, using QuantStudio 3 System
973 technology. Primers (Table S1) were designed in Primer BLAST and/or were also checked in Primer
974 BLAST for specificity to the gene of interest. Where possible, primers were chosen to cross an exon-
975 exon junction.

976 RNA expression was normalized to the internal references β-actin and/or TATAbox-binding
977 protein, from the corresponding sample (Ct_{gene}–$Ct_{reference}$=ΔCt). Furthermore, ΔCt from control samples
978 were subtracted from the ΔCt of each sample ($\Delta Ct_{treatment}$-ΔCt_{ctrl} =$\Delta\Delta Ct_{treatment}$). Fold change was
979 calculated as $2^{(-\Delta\Delta Ct)}$. These calculations were carried out using Microsoft Excel.

980
981
982

Quantification and Statistical Analysis

Data were evaluated on either on Prism version 8 for Windows or via R for Metaboanalyst generated analysis. Differences between two independent groups were compared via unpaired Student's t-test. For BCG infection studies where two independent groups were compared at several time points, multiple t-test analysis was employed, with Holm-Sidak correction for multiple comparisons. Differences were considered significant at the values of * $P < 0.05$, ** $P < 0.01$, *** $P < 0.001$ and **** $P < 0.0001$.

Data and Code Availability

All data is available at Mendeley Data DOI: 10.17632/ncbph43m85.2.

Acknowledgements

The authors would like to thank Dr Gavin McManus for his assistance with the imaging studies.

M. Lundahl was funded by a Trinity College Dublin postgraduate studentship and this work is supported by Science Foundation Ireland (SFI) Research Centre, Advanced Materials and BioEngineering Research (AMBER) under Grant number 12/RC/2278_P2 E, SFI under Grant number 12/IA/1421 and 19FFP/6484 (E. Lavelle) and SFI under Grant number 15/CDA/3310 (E. Scanlan). S. Gordon and M. Mitermite acknowledge funding from Wellcome Trust PhD Studentship 109166/Z/15/A and SFI award 15/IA/3154.

Author Contributions

M.L.E.L. performed and analyzed all experiments and wrote the paper. M.M., B.S. and S.V.G provided assistance with BCG infection studies. D.G.R, N.C.W. and L.A.J.O. assisted with Seahorse experiments. M.Y. identified and quantified the metabolites via LC-MS and D.G.R and C.F. assisted with metabolomics analysis. S.C. and F.J.S. assisted with the design and execution of the human monocyte derived macrophage experiments. R.I.L prepared samples for western blot, E.L. ran the blots and A.P.B. assisted with the experiment design and analysis. M.L.E.L., with the assistance of F.L. and A.L.G, developed the BMDM training protocol. M.L.E.L was supervised by E.M.S. and E.C.L. and the work was supervised by E.C.L.

Declaration of Interests

The authors declare no competing interests.

References

Abebe, F. (2012, September). Is interferon-gamma the right marker for bacille Calmette-Guérin-induced immune protection? The missing link in our understanding of tuberculosis immunology. *Clinical and Experimental Immunology*. Clin Exp Immunol. https://doi.org/10.1111/j.1365-2249.2012.04614.x

Aira, N., Andersson, A. M., Singh, S. K., McKay, D. M., & Blomgran, R. (2017). Species dependent impact of helminth-derived antigens on human macrophages infected with Mycobacterium tuberculosis: Direct effect on the innate anti-mycobacterial response. *PLoS Neglected Tropical Diseases*, *11*(2). https://doi.org/10.1371/journal.pntd.0005390

Amelio, P., Portevin, D., Reither, K., Mhimbira, F., Mpina, M., Tumbo, A., … Perreau, M. (2017). Mixed Th1 and Th2 Mycobacterium tuberculosis-specific CD4 T cell responses in patients with active pulmonary tuberculosis from Tanzania. *PLoS Neglected Tropical Diseases*, *11*(7). https://doi.org/10.1371/journal.pntd.0005817

Andersen, P., & Kaufmann, S. H. (2014). Novel vaccination strategies against tuberculosis. *Cold Spring Harb Perspect Med*, *4*(6). https://doi.org/10.1101/cshperspect.a018523

Arts, R. J. W., Moorlag, S. J. C. F. M., Novakovic, B., Li, Y., Wang, S. Y., Oosting, M., … Netea, M. G. (2018). BCG Vaccination Protects against Experimental Viral Infection in Humans through the Induction of Cytokines Associated with Trained Immunity. *Cell Host and Microbe*, *23*(1), 89-100.e5. https://doi.org/10.1016/j.chom.2017.12.010

Beamer, G. L., Flaherty, D. K., Assogba, B. D., Stromberg, P., Gonzalez-Juarrero, M., de Waal Malefyt, R., … Turner, J. (2008). Interleukin-10 Promotes Mycobacterium tuberculosis Disease Progression in CBA/J Mice . *The Journal of Immunology*, *181*(8), 5545–5550. https://doi.org/10.4049/jimmunol.181.8.5545

Billingham, L. K., Stoolman, J. S., Vasan, K., Rodriguez, A. E., Poor, T. A., Szibor, M., … Chandel, N. S. (2022). Mitochondrial electron transport chain is necessary for NLRP3 inflammasome activation. *Nature Immunology*, *23*(5), 692–704. https://doi.org/10.1038/S41590-022-01185-3

Bourigault, M. L., Segueni, N., Rose, S., Court, N., Vacher, R., Vasseur, V., … Quesniaux, V. F. J. (2013). Relative contribution of il-1α, il-1β and tnf to the host response to mycobacterium tuberculosis and attenuated m. Bovis bcg. *Immunity Inflammation and Disease*, *1*(1), 47–62. https://doi.org/10.1002/iid3.9

Brown, G. D., & Crocker, P. R. (2016). Lectin Receptors Expressed on Myeloid Cells. *Microbiology Spectrum*, *4*(5). https://doi.org/10.1128/microbiolspec.MCHD-0036-2016

Bystrom, J., Evans, I., Newson, J., Stables, M., Toor, I., van Rooijen, N., … Gilroy, D. W. (2008). Resolution-phase macrophages possess a unique inflammatory phenotype that is controlled by cAMP. *Blood*, *112*(10), 4117–4127. https://doi.org/10.1182/blood-2007-12-129767

Chatterjee, S., Talaat, K. R., van Seventer, E. E., Feng, C. G., Scott, A. L., Jedlicka, A., … Nutman, T. B. (2017). Mycobacteria induce TPL-2 mediated IL-10 in IL-4-generated alternatively activated macrophages. *PLoS ONE*, *12*(6). https://doi.org/10.1371/journal.pone.0179701

Cheng, S.-C., Quintin, J., Cramer, R. A., Shepardson, K. M., Saeed, S., Kumar, V., … Netea, M. G. (2014). mTOR- and HIF-1α-mediated aerobic glycolysis as metabolic basis for trained immunity. *Science (New York, N.Y.)*, *345*(6204), 1250684. https://doi.org/10.1126/science.1250684

Cohen, S. B., Gern, B. H., Delahaye, J. L., Adams, K. N., Plumlee, C. R., Winkler, J. K., … Urdahl, K. B. (2018). Alveolar Macrophages Provide an Early Mycobacterium tuberculosis Niche and Initiate Dissemination. *Cell Host & Microbe*, *24*(3), 439–446. https://doi.org/10.1016/j.chom.2018.08.001

1059 Cumming, B. M., Addicott, K. W., Adamson, J. H., & Steyn, A. J. C. (2018). Mycobacterium tuberculosis
1060 induces decelerated bioenergetic metabolism in human macrophages. *ELife*, *7*.
1061 https://doi.org/10.7554/eLife.39169

1062 Ferrante, C. J., & Leibovich, S. J. (2012). Regulation of Macrophage Polarization and Wound Healing.
1063 In *Adv Wound Care (New Rochelle)* (Vol. 1, pp. 10–16). Department of Cell Biology and Molecular
1064 Medicine and The Cardiovascular Research Institute, New Jersey Medical School, University of
1065 Medicine and Dentistry of New Jersey , Newark, New Jersey.
1066 https://doi.org/10.1089/wound.2011.0307

1067 Flynn, J. L., Chan, J., Triebold, K. J., Dalton, D. K., Stewart, T. A., & Bloom, B. R. (1993). An essential role
1068 for interferon gamma in resistance to Mycobacterium tuberculosis infection. *J Exp Med*, *178*(6),
1069 2249–2254.

1070 Gabrilovich, D. I., Ostrand-Rosenberg, S., & Bronte, V. (2012). Coordinated regulation of myeloid cells
1071 by tumours. *Nature Reviews Immunology*, *12*(4), 253–268. https://doi.org/10.1038/nri3175

1072 Gause, W. C., Wynn, T. A., & Allen, J. E. (2013, August 5). Type 2 immunity and wound healing:
1073 Evolutionary refinement of adaptive immunity by helminths. *Nature Reviews Immunology*.
1074 Nature Publishing Group. https://doi.org/10.1038/nri3476

1075 Gleeson, L. E., Sheedy, F. J., Palsson-McDermott, E. M., Triglia, D., O'Leary, S. M., O'Sullivan, M. P., …
1076 Keane, J. (2016). Cutting Edge: Mycobacterium tuberculosis Induces Aerobic Glycolysis in Human
1077 Alveolar Macrophages That Is Required for Control of Intracellular Bacillary Replication . *The*
1078 *Journal of Immunology*, *196*(6), 2444–2449. https://doi.org/10.4049/jimmunol.1501612

1079 Gordon, S., & Martinez, F. O. (2010). Alternative activation of macrophages: mechanism and functions.
1080 *Immunity*, *32*(5), 593–604. https://doi.org/10.1016/j.immuni.2010.05.007

1081 Hackett, E. E., Charles-Messance, H., O'Leary, S. M., Gleeson, L. E., Muñoz-Wolf, N., Case, S., … Sheedy,
1082 F. J. (2020). Mycobacterium tuberculosis Limits Host Glycolysis and IL-1β by Restriction of PFK-M
1083 via MicroRNA-21. *Cell Reports*, *30*(1), 124-136.e4. https://doi.org/10.1016/j.celrep.2019.12.015

1084 Huang, L., Nazarova, E. V., & Russell, D. G. (2019). Mycobacterium tuberculosis: Bacterial Fitness within
1085 the Host Macrophage. In *Bacteria and Intracellularity* (Vol. 7, pp. 127–138). American Society of
1086 Microbiology. https://doi.org/10.1128/microbiolspec.bai-0001-2019

1087 Huang, L., Nazarova, E. V., Tan, S., Liu, Y., & Russell, D. G. (2018). Growth of Mycobacterium
1088 tuberculosis in vivo segregates with host macrophage metabolism and ontogeny. *Journal of*
1089 *Experimental Medicine*, *215*(4), 1135–1152. https://doi.org/10.1084/jem.20172020

1090 Jouanguy, E., Lamhamedi-Cherradi, S., Lammas, D., Dorman, S. E., Fondanèche, M. C., Dupuis, S., …
1091 Casanova, J. L. (1999). A human IFNGR1 small deletion hotspot associated with dominant
1092 susceptibility to mycobacterial infection. *Nature Genetics*, *21*(4), 370–378.
1093 https://doi.org/10.1038/7701

1094 Kahnert, A., Seiler, P., Stein, M., Bandermann, S., Hahnke, K., Mollenkopf, H., & Kaufmann, S. H. E.
1095 (2006). Alternative activation deprives macrophages of a coordinated defense program to
1096 Mycobacterium tuberculosis. *European Journal of Immunology*, *36*(3), 631–647.
1097 https://doi.org/10.1002/eji.200535496

1098 Keane, J., Gershon, S., Wise, R. P., Mirabile-Levens, E., Kasznica, J., Schwieterman, W. D., … Braun, M.
1099 M. (2001). Tuberculosis Associated with Infliximab, a Tumor Necrosis Factor α–Neutralizing
1100 Agent. *New England Journal of Medicine*, *345*(15), 1098–1104.
1101 https://doi.org/10.1056/nejmoa011110

1102 Khader, S. A., Divangahi, M., Hanekom, W., Hill, P. C., Maeurer, M., Makar, K. W., … Bill and Melinda
1103 Gates Foundation Collaboration for TB Vaccine Discovery Innate Immunity Working Group18.
1104 (2019). Targeting innate immunity for tuberculosis vaccination. *Journal of Clinical Investigation*,

129(9), 3482–3491. https://doi.org/10.1172/JCI128877

Khan, A., Singh, V. K., Hunter, R. L., & Jagannath, C. (2019, August 1). Macrophage heterogeneity and plasticity in tuberculosis. *Journal of Leukocyte Biology*. John Wiley and Sons Inc. https://doi.org/10.1002/JLB.MR0318-095RR

Khan, N., Downey, J., Sanz, J., Kaufmann, E., Blankenhaus, B., Pacis, A., … Divangahi, M. (2020). M. tuberculosis Reprograms Hematopoietic Stem Cells to Limit Myelopoiesis and Impair Trained Immunity. *Cell*, *183*(3), 752-770.e22. https://doi.org/10.1016/j.cell.2020.09.062

Kleinnijenhuis, J., Quintin, J., Preijers, F., Joosten, L. A. B., Ifrim, D. C., Saeed, S., … Netea, M. G. (2012). Bacille Calmette-Guerin induces NOD2-dependent nonspecific protection from reinfection via epigenetic reprogramming of monocytes. *Proceedings of the National Academy of Sciences of the United States of America*, *109*(43), 17537–17542. https://doi.org/10.1073/pnas.1202870109

Lebre, F., Hanlon, D., Boland, J. B., Coleman, J., & Lavelle, E. C. (2018). Exfoliation in Endotoxin-Free Albumin Generates Pristine Graphene with Reduced Inflammatory Properties. *Advanced Biosystems*, *2*(12), 1800102 (1-15). https://doi.org/10.1002/adbi.201800102

Li, L., Ng, D. S. W., Mah, W. C., Almeida, F. F., Rahmat, S. A., Rao, V. K., … Lane, D. P. (2015). A unique role for p53 in the regulation of M2 macrophage polarization. *Cell Death and Differentiation*, *22*(7), 1081–1093. https://doi.org/10.1038/cdd.2014.212

Li, X. X., & Zhou, X. N. (2013). Co-infection of tuberculosis and parasitic diseases in humans: A systematic review. *Parasites and Vectors*. Parasit Vectors. https://doi.org/10.1186/1756-3305-6-79

Liu, L., Lu, Y., Martinez, J., Bi, Y., Lian, G., Wang, T., … Wang, R. (2016). Proinflammatory signal suppresses proliferation and shifts macrophage metabolism from Myc-dependent to HIF1α-dependent. *Proceedings of the National Academy of Sciences of the United States of America*, *113*(6), 1564–1569. https://doi.org/10.1073/pnas.1518000113

Luiz, J. P. M., Toller-Kawahisa, J. E., Viacava, P. R., Nascimento, D. C., Pereira, P. T., Saraiva, A. L., … Alves-Filho, J. C. (2020). MEK5/ERK5 signaling mediates IL-4-induced M2 macrophage differentiation through regulation of c-Myc expression. *Journal of Leukocyte Biology*, *108*(4), 1215–1223. https://doi.org/10.1002/JLB.1MA0520-016R

Lundahl, M. L. E., Scanlan, E. M., & Lavelle, E. C. (2017). Therapeutic potential of carbohydrates as regulators of macrophage activation. *Biochemical Pharmacology*, *146*, 23–41. https://doi.org/10.1016/j.bcp.2017.09.003

Lundahl, M., Lynch, D. M., Barnes, D., McSweeney, L., Gorman, A., Lebre, F., … Scanlan, E. M. (2020). Mycobacterial para-Hydroxybenzoic Acid-Derivatives (pHBADs) and Related Structures Induce Macrophage Innate Memory. *ACS Chemical Biology*, *15*(9), 2415–2421. https://doi.org/10.1021/acschembio.0c00378

Mabbott, N. A. (2018). The Influence of Parasite Infections on Host Immunity to Co-infection With Other Pathogens. *Frontiers in Immunology*. NLM (Medline). https://doi.org/10.3389/fimmu.2018.02579

Mantovani, A., Sica, A., Sozzani, S., Allavena, P., Vecchi, A., & Locati, M. (2004). The chemokine system in diverse forms of macrophage activation and polarization. *Trends Immunol*, *25*(12), 677–686. https://doi.org/10.1016/j.it.2004.09.015

Monin, L., Griffiths, K. L., Lam, W. Y., Gopal, R., Kang, D. D., Ahmed, M., … Khader, S. A. (2015). Helminth-induced arginase-1 exacerbates lung inflammation and disease severity in tuberculosis. *Journal of Clinical Investigation*, *125*(12), 4699–4713. https://doi.org/10.1172/JCI77378

1150 Moorlag, S. J. C. F. M., Khan, N., Novakovic, B., Kaufmann, E., Jansen, T., van Crevel, R., … Netea, M. G.
1151 (2020). β-Glucan Induces Protective Trained Immunity against Mycobacterium tuberculosis
1152 Infection: A Key Role for IL-1. *Cell Reports*, *31*(7). https://doi.org/10.1016/j.celrep.2020.107634

1153 Moreira-Teixeira, L., Sousa, J., McNab, F. W., Torrado, E., Cardoso, F., Machado, H., … Saraiva, M.
1154 (2016). Type I IFN Inhibits Alternative Macrophage Activation during Mycobacterium
1155 tuberculosis Infection and Leads to Enhanced Protection in the Absence of IFN-γ Signaling.
1156 *Journal of Immunology (Baltimore, Md. : 1950)*, *197*(12), 4714–4726.
1157 https://doi.org/10.4049/jimmunol.1600584

1158 Murray, P. J., & Wynn, T. A. (2011). Protective and pathogenic functions of macrophage subsets.
1159 *Nature Reviews Immunology*, *11*(11), 723–737. https://doi.org/10.1038/nri3073

1160 O'Leary, S., O'Sullivan, M. P., & Keane, J. (2011). IL-10 blocks phagosome maturation in mycobacterium
1161 tuberculosis-infected human macrophages. *Am J Respir Cell Mol Biol*, *45*(1), 172–180.
1162 https://doi.org/10.1165/rcmb.2010-0319OC

1163 O'Neill, L. A. J., Kishton, R. J., & Rathmell, J. (2016). A guide to immunometabolism for immunologists.
1164 *Nature Reviews Immunology 2016 16:9*, *16*(9), 553–565. https://doi.org/10.1038/NRI.2016.70

1165 O'Shea, M. K., Fletcher, T. E., Muller, J., Tanner, R., Matsumiya, M., Bailey, J. W., … McShane, H. (2018).
1166 Human Hookworm Infection Enhances Mycobacterial Growth Inhibition and Associates With
1167 Reduced Risk of Tuberculosis Infection. *Frontiers in Immunology*, *9*, 2893.
1168 https://doi.org/10.3389/fimmu.2018.02893

1169 Ottenhoff, T. H. M., Doherty, T. M., Van Dissel, J. T., Bang, P., Lingnau, K., Kromann, I., & Andersen, P.
1170 (2010, December). First in humans: A new molecularly defined vaccine shows excellent safety
1171 and strong induction of long-lived Mycobacterium tuberculosis-specific Th1-cell like responses.
1172 *Human Vaccines*. Hum Vaccin. https://doi.org/10.4161/hv.6.12.13143

1173 Palsson-McDermott, E. M., Curtis, A. M., Goel, G., Lauterbach, M. A. R., Sheedy, F. J., Gleeson, L. E., …
1174 O'Neill, L. A. J. (2015). Pyruvate Kinase M2 Regulates Hif-1α Activity and IL-1β Induction and Is a
1175 Critical Determinant of the Warburg Effect in LPS-Activated Macrophages. *Cell Metabolism*,
1176 *21*(1), 65–80. https://doi.org/10.1016/j.cmet.2014.12.005

1177 Pasula, R., Martin, W. J., Kesavalu, B. R., Abdalla, M. Y., & Britigan, B. E. (2017). Passive transfer of
1178 interferon-γ over-expressing macrophages enhances resistance of SCID mice to Mycobacterium
1179 tuberculosis infection. *Cytokine*, *95*, 70–79. https://doi.org/10.1016/j.cyto.2017.02.009

1180 Philips, J. A., & Ernst, J. D. (2012). Tuberculosis pathogenesis and immunity. *Annu Rev Pathol*, *7*, 353–
1181 384. https://doi.org/10.1146/annurev-pathol-011811-132458

1182 Potian, J. A., Rafi, W., Bhatt, K., McBride, A., Gause, W. C., & Salgame, P. (2011). Preexisting helminth
1183 infection induces inhibition of innate pulmonary anti-tuberculosis defense by engaging the IL-4
1184 receptor pathway. *Journal of Experimental Medicine*, *208*(9), 1863–1874.
1185 https://doi.org/10.1084/jem.20091473

1186 Quinn, S. M., Cunningham, K., Raverdeau, M., Walsh, R. J., Curham, L., Malara, A., & Mills, K. H. G.
1187 (2019). Anti-inflammatory trained immunity mediated by helminth products attenuates the
1188 induction of T cell-mediated autoimmune disease. *Frontiers in Immunology*, *10*(MAY).
1189 https://doi.org/10.3389/fimmu.2019.01109

1190 Quintin, J., Saeed, S., Martens, J. H. A., Giamarellos-Bourboulis, E. J., Ifrim, D. C., Logie, C., … Netea, M.
1191 G. (2012). Candida albicans infection affords protection against reinfection via functional
1192 reprogramming of monocytes. *Cell Host & Microbe*, *12*(2), 223–232.
1193 https://doi.org/10.1016/j.chom.2012.06.006

1194 Roy, S., Mukhopadhyay, D., Mukherjee, S., Moulik, S., Chatterji, S., Brahme, N., … Chatterjee, M.
1195 (2018). An IL-10 dominant polarization of monocytes is a feature of Indian Visceral Leishmaniasis.

Parasite Immunology, *40*(7). https://doi.org/10.1111/pim.12535

Saeed, S., Quintin, J., Kerstens, H. H. D., Rao, N. A., Aghajanirefah, A., Matarese, F., … Stunnenberg, H. G. (2014). Epigenetic programming of monocyte-to-macrophage differentiation and trained innate immunity. *Science (New York, N.Y.)*, *345*(6204), 1251086. https://doi.org/10.1126/science.1251086

Salgame, P., Yap, G. S., & Gause, W. C. (2013). Effect of helminth-induced immunity on infections with microbial pathogens. *Nature Immunology*. Nat Immunol. https://doi.org/10.1038/ni.2736

Seth, P., Csizmadia, E., Hedblom, A., Vuerich, M., XIE, H., Li, M., … Wegiel, B. (2017). Deletion of lactate dehydrogenase-A in myeloid cells triggers antitumor immunity. *Cancer Research*, canres.2938.2016. https://doi.org/10.1158/0008-5472.CAN-16-2938

Shi, L., Jiang, Q., Bushkin, Y., Subbian, S., & Tyagi, S. (2019). Biphasic dynamics of macrophage immunometabolism during Mycobacterium tuberculosis infection. *MBio*, *10*(2). https://doi.org/10.1128/mBio.02550-18

Sica, A., Erreni, M., Allavena, P., & Porta, C. (2015). Macrophage polarization in pathology. *Cellular and Molecular Life Sciences*, *72*(21), 4111–4126. https://doi.org/10.1007/s00018-015-1995-y

Timblin, G. A., Tharp, K. M., Ford, B., Winchester, J. M., Wang, J., Zhu, S., … Saijo, K. (2021). Mitohormesis reprogrammes macrophage metabolism to enforce tolerance. *Nature Metabolism*, *3*(5), 618–635. https://doi.org/10.1038/S42255-021-00392-W

Van den Bossche, J., Baardman, J., Otto, N. A., van der Velden, S., Neele, A. E., van den Berg, S. M., … de Winther, M. P. J. (2016). Mitochondrial Dysfunction Prevents Repolarization of Inflammatory Macrophages. *Cell Reports*, *17*(3), 684–696. https://doi.org/10.1016/j.celrep.2016.09.008

Van den Bossche, J., O'Neill, L. A., & Menon, D. (2017). Macrophage Immunometabolism: Where Are We (Going)? *Trends in Immunology*. https://doi.org/10.1016/j.it.2017.03.001

van der Meer, J. W. M., Joosten, L. A. B., Riksen, N., & Netea, M. G. (2015). Trained immunity: A smart way to enhance innate immune defence. *Molecular Immunology*, *68*(1), 40–44. https://doi.org/10.1016/j.molimm.2015.06.019

Viola, A., Munari, F., Sánchez-Rodríguez, R., Scolaro, T., & Castegna, A. (2019). The metabolic signature of macrophage responses. *Frontiers in Immunology*, *10*(JULY). https://doi.org/10.3389/fimmu.2019.01462

Wang, F., Zhang, S., Vuckovic, I., Jeon, R., Lerman, A., Folmes, C. D., … Herrmann, J. (2018). Glycolytic Stimulation Is Not a Requirement for M2 Macrophage Differentiation. *Cell Metabolism*, *28*(3), 463-475.e4. https://doi.org/10.1016/j.cmet.2018.08.012

World Health Organization. (2021). Global Tuberculosis Report 2021. *Global Tuberculosis Report*, 1–57. Retrieved from http://apps.who.int/bookorders.

Supplemental Information

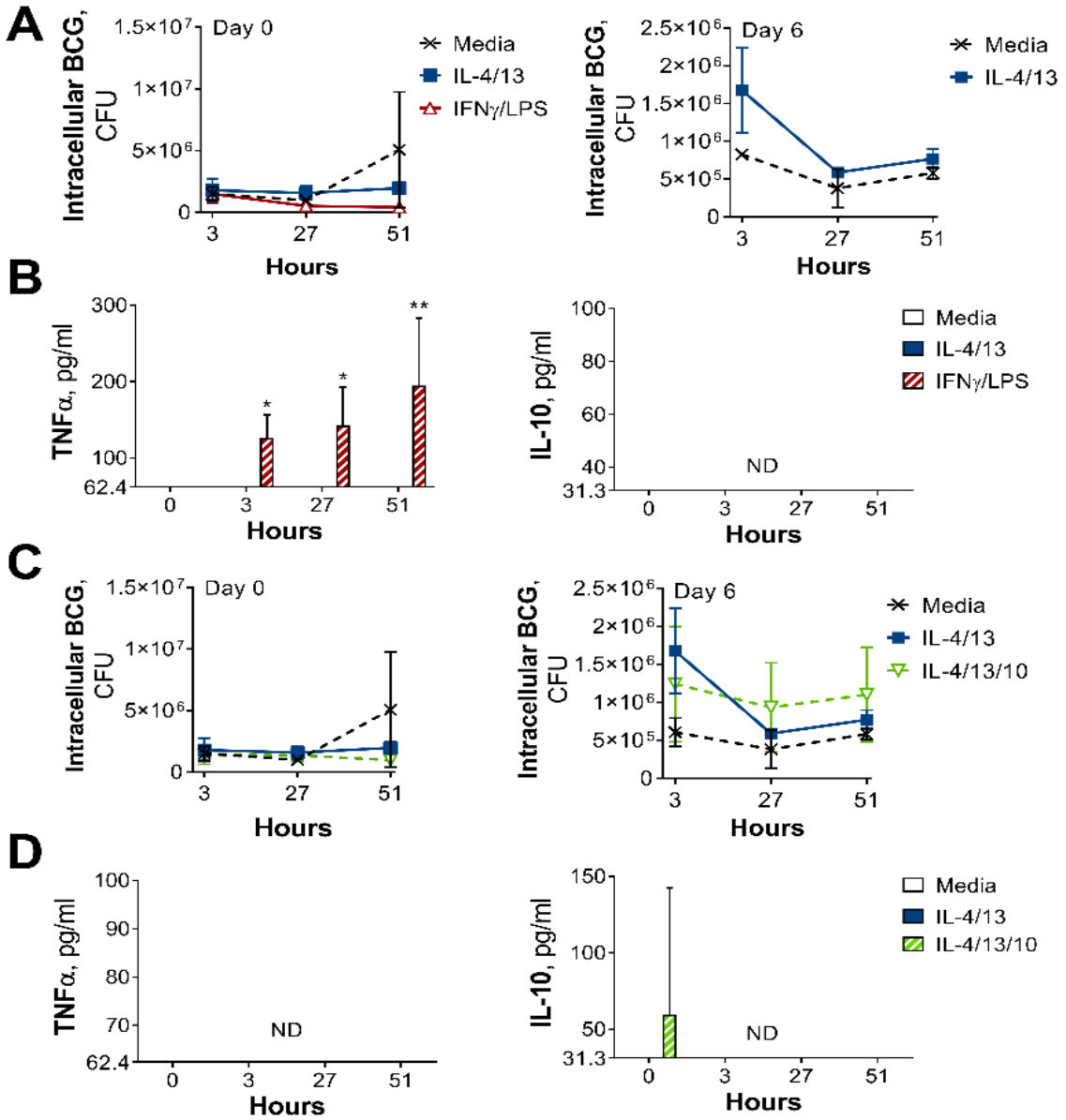

Figure S1. CFU counts and cytokine secretion from BCG killing experiments.

(**A-B**) BCG Denmark CFU counts (A) and cytokine secretion (B) on Day 0 or Day 6 after h following BMDM BCG infection. BMDMs were previously incubated with media control, IL-4 with IL-13 or IFNγ with LPS for 24 h on Day -1. Representative results (n = 2 out of ≥ 3), standardized to 0.5 × 10^6 cells, shown as mean ± SEM (A-B) and analyzed by multiple t-test, with Holm-Sidak correction, compared with media control (B). (**C-D**) BCG Denmark CFU counts (C) and cytokine secretion (D) on Day 0 or Day 6 after h following BMDM BCG infection. BMDMs were previously incubated with media control or IL-4 and IL-13, with or without IL-10, for 24 h on Day -1. Representative results (n = 2 out of ≥ 3), standardized to 0.5 × 10^6 cells, shown as mean ± SEM (C-D) and analyzed by multiple t-test, with Holm-Sidak correction, compared with media control (D). * $p \leq 0.05$, ** $p \leq 0.01$.

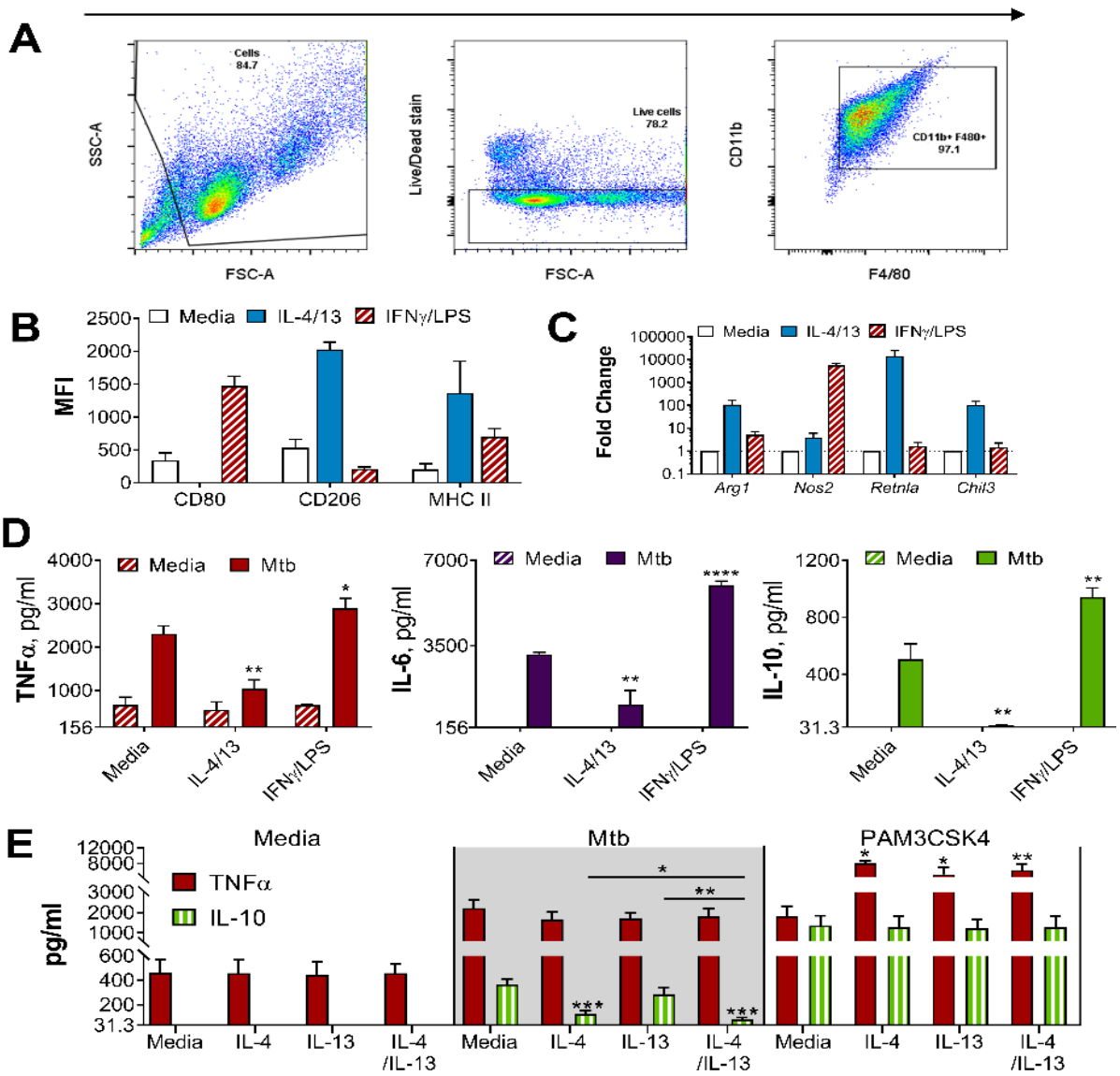

Figure S2. BMDMs either classically activated with IFNγ and LPS or alternatively activated with IL-4 and IL-13.

(**A**) Gating strategy for flow cytometry analysis, gating on cells, live cells and CD11b+ F480+ BMDMs. (**B**) Surface marker expression of CD80, CD206 and MHC II on BMDMs incubated with media as a control, IL-4 with IL-13 or IFNγ with LPS for 24 h (n = 3). (**C**) qPCR of indicated mRNA in BMDMs treated as in (B), standardized to media control (n = 4). (**D-E**) Cytokine secretion from BMDMs incubated with media, IL-4, IL-13, IL-4 with IL-13 or IFNγ with LPS for 24 h on Day -1 and stimulated with media, irradiated *M. tuberculosis* H37Rv (Mtb) or PAM3CSK4 for 24 h on Day 6 (n = 3). Mean ± SD are shown and analyzed by student's t-test, compared to media control or as indicated. * $p \leq 0.05$, ** $p \leq 0.01$, *** $p \leq 0.001$, **** $p \leq 0.0001$.

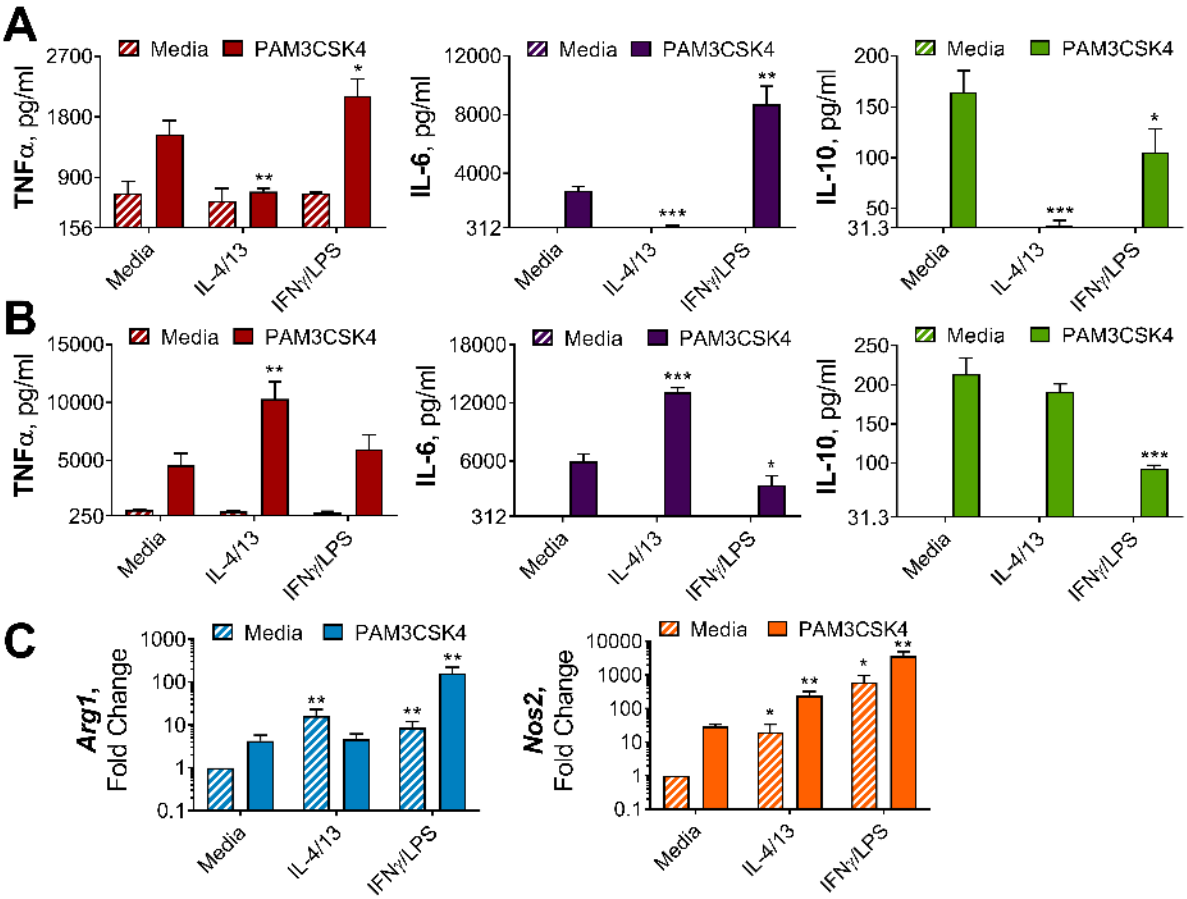

1259

1260 **Figure S3. IL-4 and IL-13 innate training enhances inflammatory and bactericidal responses following**
1261 **TLR 1/2 stimulation**

1262 (**A-B**) Cytokine secretion from BMDMs following incubation with media control, IL-4 with IL-13 or IFNγ with LPS
1263 for 24 h on Day -1 and incubated with media or PAM3CSK4 on Day 0 (A) or Day 6 (B) for 24 hours (n = 3). (**C**)
1264 qPCR of indicated mRNA in BMDMs treated as in (B), standardized to BMDMs incubated with media Day -1 and
1265 Day 6 (n = 4). Mean ± SD are shown and analyzed by student's t-test, compared with media control. * $p \leq 0.05$,
1266 ** $p \leq 0.01$, *** $p \leq 0.001$.
1267

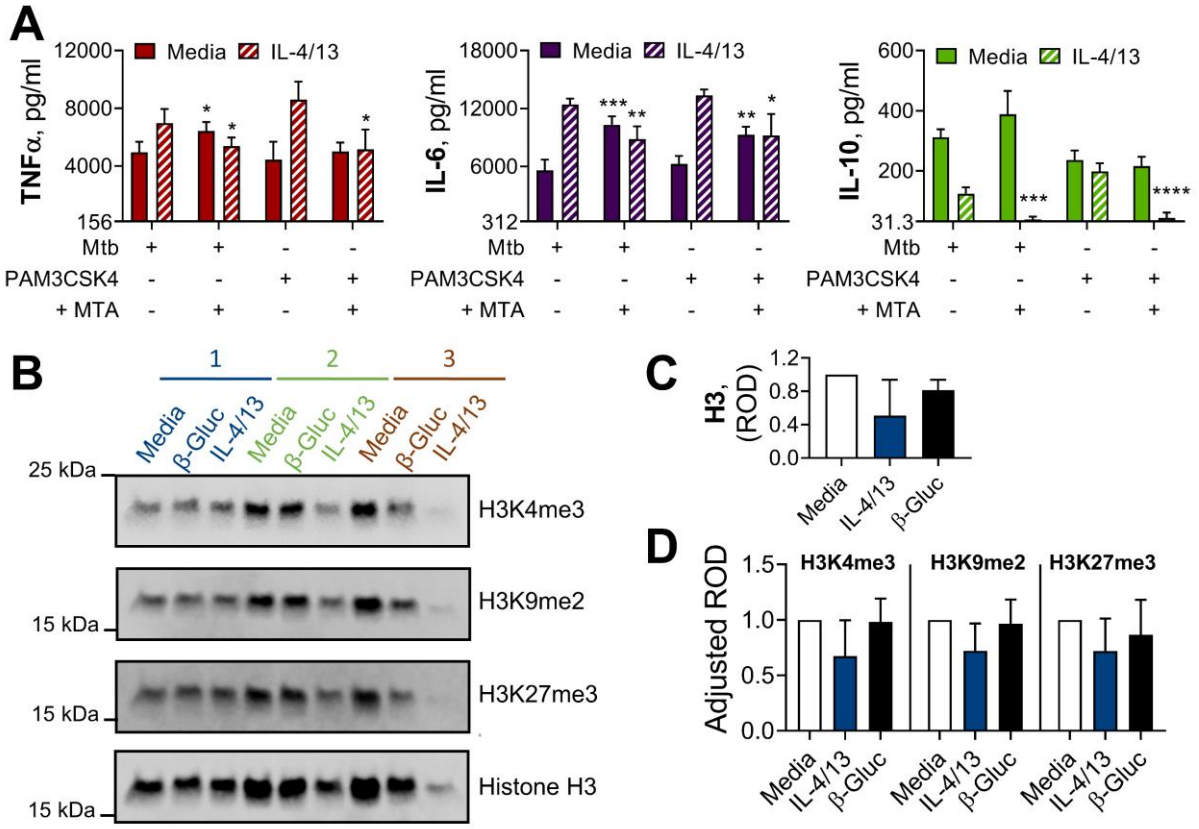

Figure S4. Methylation contributes to IL-4 and IL-13 innate training.

(**A**) Cytokine secretion following BMDM incubation with media control or IL-4 with IL-13 for 24 h on Day -1, with or without 1 hour pre-incubation with methylation inhibitor MTA, and incubation with irradiated *M. tuberculosis* H37Rv (Mtb) or PAM3CSK4 for 24 h on Day 6 (n = 4). (**B-D**) Protein extract (B) and densitometry values (C-D) from western blot analysis of histone methylation in BMDMs incubated with media control, yeast β-glucan (β-Gluc) or IL-4 with IL-13 on Day -1 and lysed on Day 6 (n = 3). (A, C-D) Mean ± SD are shown and analyzed by student's t-test, comparing with or without MTA (A) or with media control (C-D). * $p \leq 0.05$, ** $p \leq 0.01$, *** $p \leq 0.001$, **** $p \leq 0.0001$.

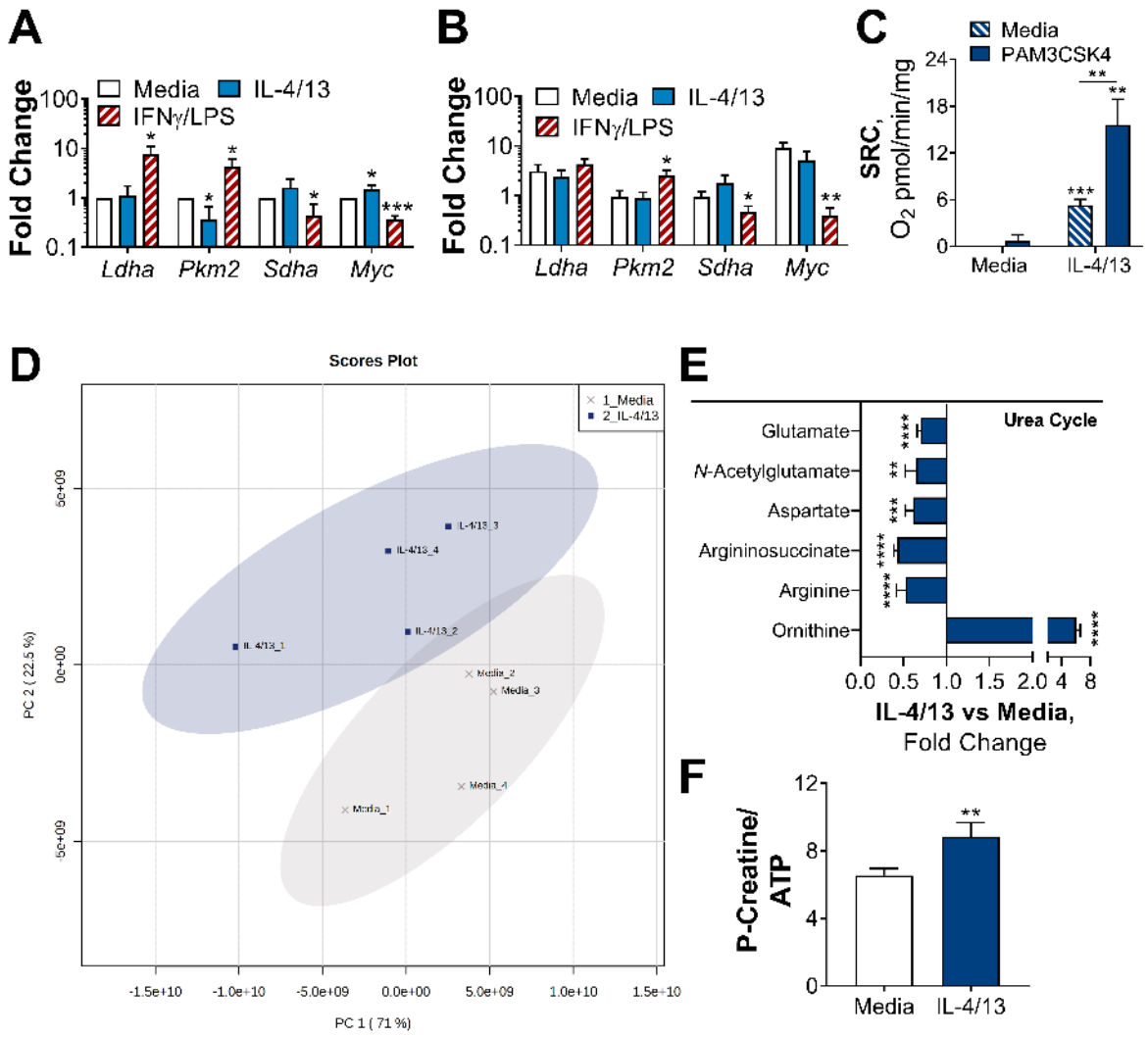

Figure S5. Challenged BMDMs previously trained with IL-4 and IL-13 retain M2-typical metabolism.

(**A-B**) qPCR of indicated mRNA in BMDMs following incubation with media control, IL-4 with IL-13 or IFNγ with LPS on for 24 h Day -1 and stimulated with media (A) or PAM3CSK4 (B) on Day 6 for 6 h (*Pkm2*) and 24 h (*Ldha, Sdha* and *Myc*). Fold change was standardized to BMDMs incubated with media Day -1 and Day 6 (n = 3). (**C**) Spare respiratory capacity (SRC) of BMDMs treated as in (A-B), with incubation of media or IL-4 with IL-13 on Day -1 (n = 3). (**D-F**) Metabolites isolated from BMDMs following incubation with either media control (untrained) or IL-4 with IL-13 (trained) for 24 h on Day -1 and stimulation with Mtb for 24 h on Day 6 (n = 4). Metaboanalyst principal component analysis (PCA) (D), fold change of metabolites from trained BMDMs compared with media control (=1) (E) and calculated ratio of phosphocreatine (P-creatine) to ATP (F) are shown. Mean ± SD are shown and analyzed by student t-test, compared with media control. * $p \leq 0.05$, ** $p \leq 0.01$, *** $p \leq 0.001$, **** $p \leq 0.0001$.

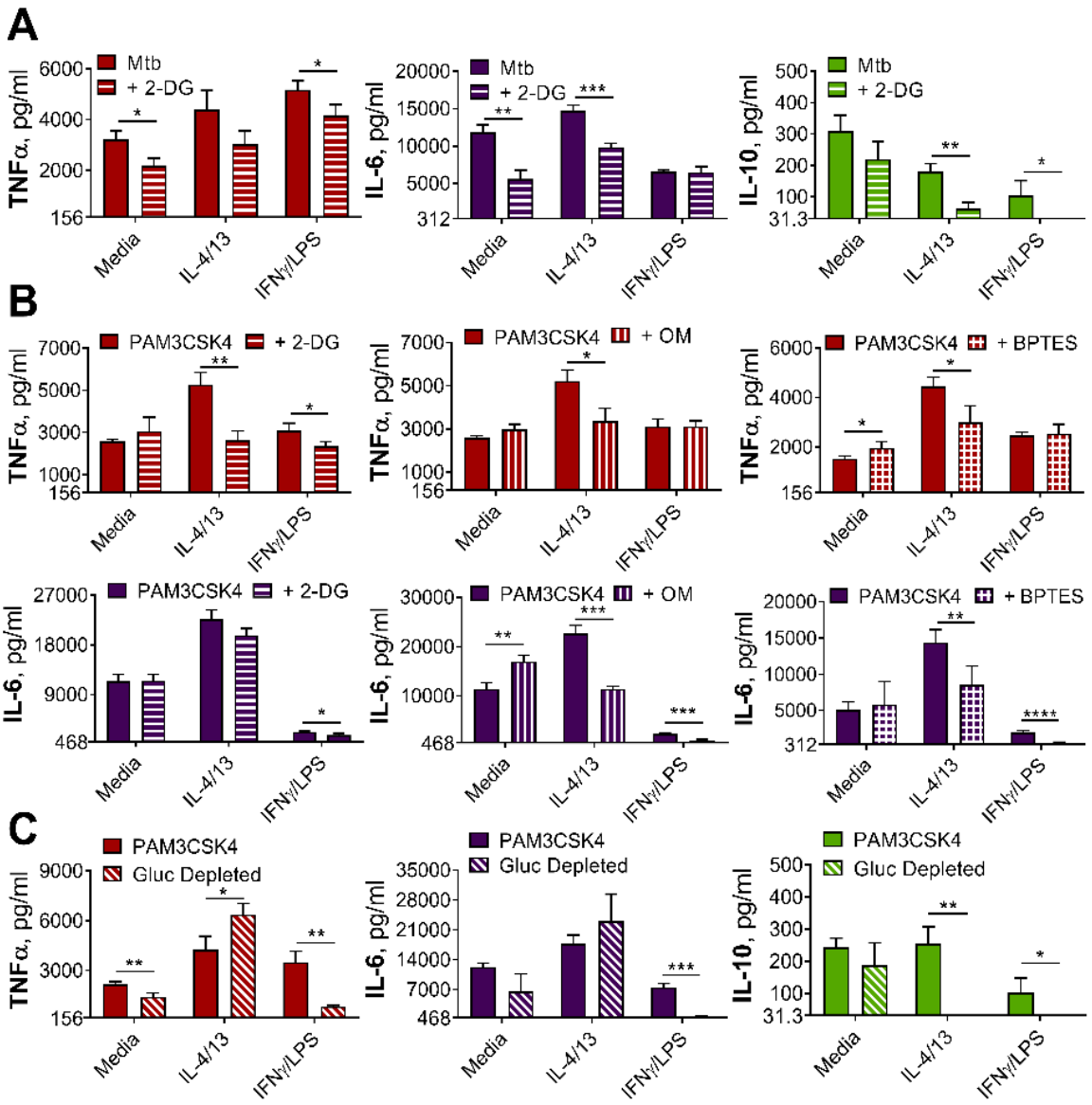

1291

1292 **Figure S6. Innate training with IL-4 and IL-13 enhancement of pro-inflammatory responses is not**
1293 **dependent upon glucose metabolism.**

1294 (**A-B**) Cytokine secretion from BMDMs following incubation with media control, IL-4 with IL-13 or IFNγ with LPS
1295 for 24 h on Day -1 and incubation with irradiated *M. tuberculosis* H37Rv (Mtb) (A) or PAM3CSK4 (B) for 24 h on
1296 Day 6, with or without pre-incubation of metabolic inhibitors oligomycin (OM), 2-deoxy glucose (2-DG) or BPTES.
1297 (**C**) Cytokine secretion from BMDMs following incubation with media control, IL-4 with IL-13 or IFNγ with LPS for
1298 24 h on Day -1 and incubation with media or PAM3CSK4 for 24 h on Day 6, with or without glucose depleted
1299 conditions between Day -1 to 7. Mean ± SD (n = 3-4) are shown and analyzed by student's t-test as indicated. *
1300 $p \leq 0.05$, ** $p \leq 0.01$, *** $p \leq 0.001$, **** $p \leq 0.0001$.
1301

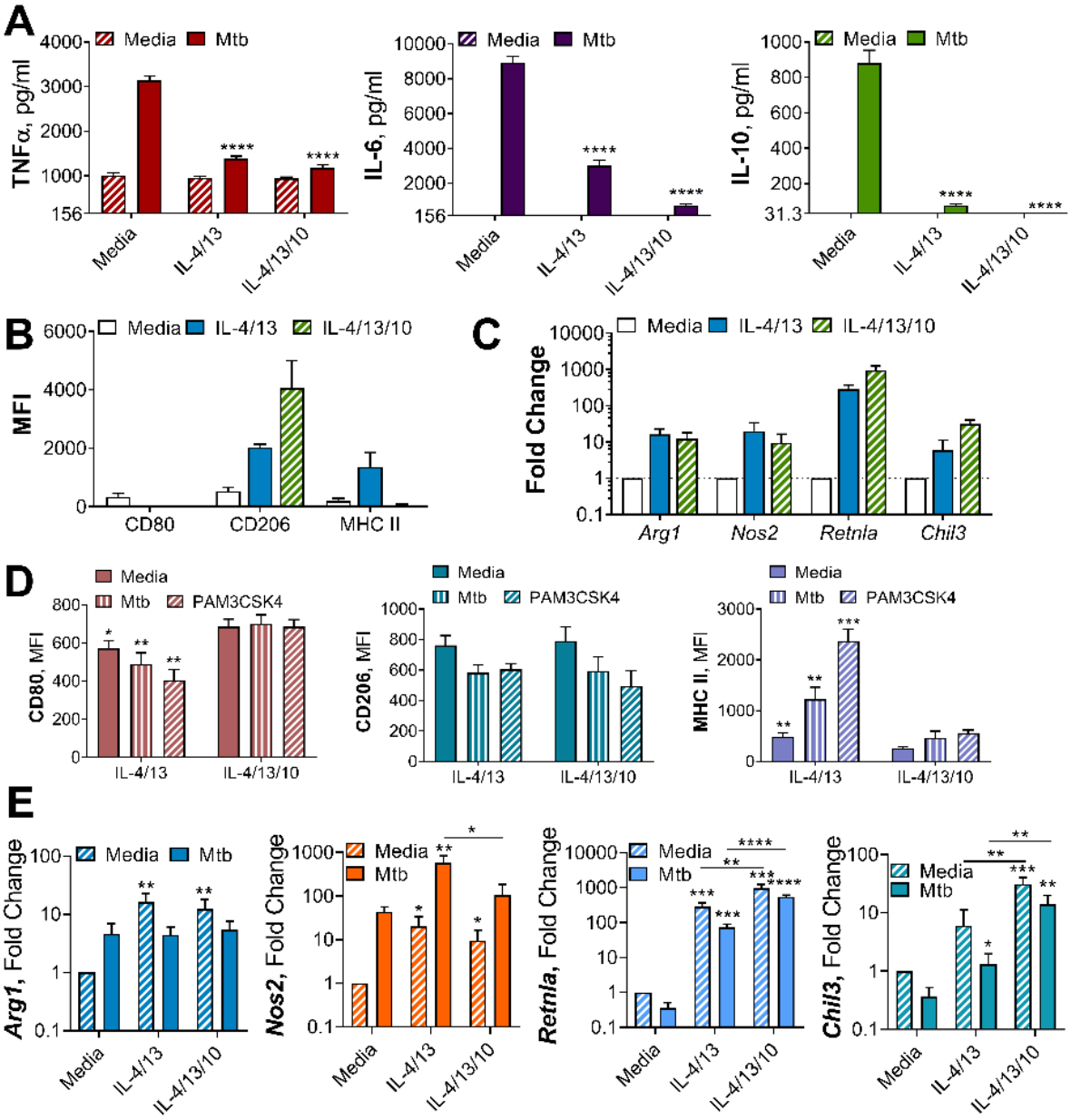

Figure S7. Alternative macrophage activation with or without IL-10.

(**A**) Cytokine secretion from BMDMs incubated with media as a control or IL-4 and IL-13, with or without IL-10 for 24 h on Day-1, then incubated with media or Mtb for 24 h on Day 0 (n = 4). (**B**) Surface marker expression of CD80, CD206 and MHC II on BMDMs incubated with media as a control or IL-4 and IL-13, with or without IL-10 for 24 h (n = 3) (gating strategy shown Figure S2A). (**C**) qPCR of indicated mRNA in BMDMs treated as in (B), standardized to media control (n = 4). (**D**) Surface marker expression of CD80, CD206 and MHC II on BMDMs following incubation with IL-4 and IL-13, with or without IL-10, for 24 h on Day -1 and incubated with media, irradiated *M. tuberculosis* H37Rv (Mtb) or PAM3CSK4 for 24 h on Day 0 (n =3). (**E**) qPCR of indicated mRNA in BMDMs treated as in (A), standardized to BMDM incubated with media on Day -1 and Day 0 (n = 4). Mean ± SD are shown (A-E) and analyzed by student's t-test, compared with media control (A, E), comparing with or without IL-10 (D, E). * $p \leq 0.05$, ** $p \leq 0.01$, *** $p \leq 0.001$, **** $p \leq 0.0001$.

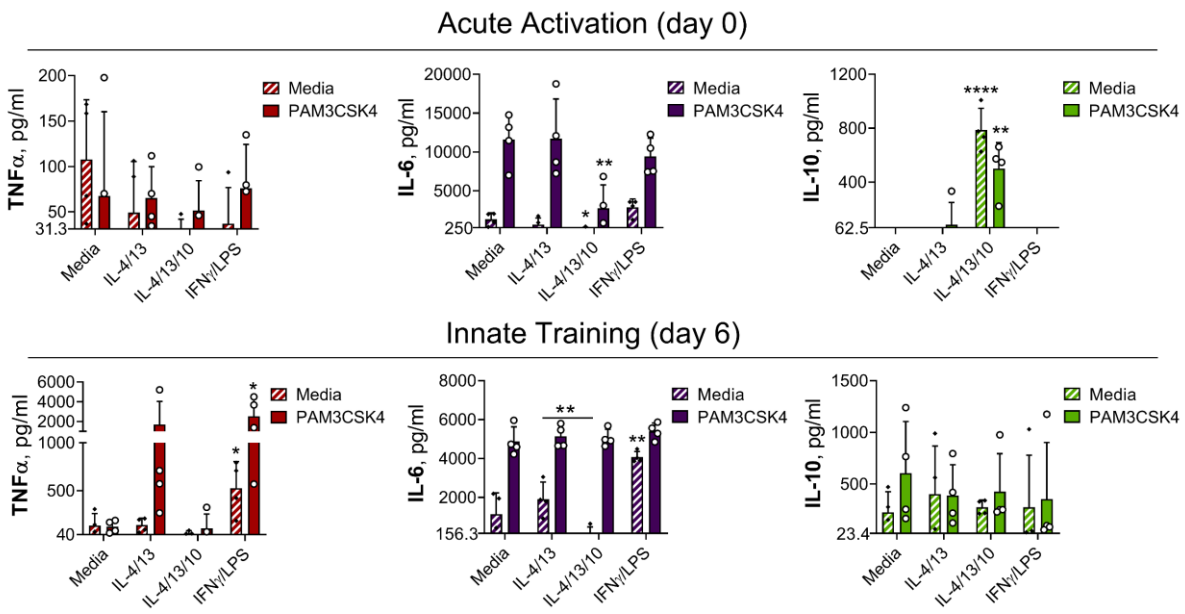

Figure S8. IL-4 and IL-13 innate training alters MoDM responses following PAM3CSK4 stimulation
Cytokine secretion following MoDM 24 h incubation with PAM3CSK4 or media on Day 0 or on Day 6 as indicated. MoDM were previously incubated with media, IL-4 with IL-13 – with or without the addition of IL-10 – or IFNγ with LPS on Day -1 for 24 h (n = 4, each rep shown by a symbol). Mean ± SD are shown and analyzed by student's t-test, compared with media control or comparing IL-4/IL-13 training with or without IL-10, as indicated. * $p \leq 0.05$, ** $p \leq 0.01$, **** $p \leq 0.0001$.

1336 **Table S 1. Primer sequences for reverse transcription PCR.**

Primer		Source
Actb (RefSeq: NM_007393.5)	FP: GCTTCTTTGCAGCTCCTTCGT	Invitrogen Custom DNA Oligos
	RP: CGTCATCCATGGCGAACTG	
Arg1 (RefSeq: NM_007482.3)	FP: TACAAGACAGGGCTCCTTTCAG	Invitrogen Custom DNA Oligos
	RP: TGAGTTCCGAAGCAAGCCAA	
Chitl3 (RefSeq: NM_009892.3)	FP: AAGCTCTCCAGAAGCAATCC	Invitrogen Custom DNA Oligos
	RP: AGAAGAATTGCCAGACCTGTGA	
Ldha (RefSeq: NM_010699.2, NM_001136069.2)	FP: GAGACTTGGCTGAGAGCATAA	Eurofins genomics (MWG)
	RP: GATACATGGGACACTGAGGAA	
Myc (RefSeq: NM_010849.4)	FP: CAGCGACTCTGAAGAAGAGCA	Invitrogen Custom DNA Oligos
	RP: GACCTCTTGGCAGGGGTTTG	
Nos2 (RefSeq: NM_010927.4, NM_001313921.1, NM_001313922.1)	FP: TCCTGGACATTACGACCCCT	Invitrogen Custom DNA Oligos
	RP: CTCTGAGGGCTGACACAAGG	
Pkm2 (RefSeq: NM_011099.4, NM_001378868.1, NM_001378869.1, NM_001378870.1)	FP: TGTCTGGAGAAACAGCCAAG	Eurofins genomics (MWG)
	RP: CGAATAGCTGCAAGTGGTAGA	
Retnla (RefSeq: NM_020509.3)	FP: CAGCTGATGGTCCCAGTGAAT	Invitrogen Custom DNA Oligos
	RP: AGTGGAGGGATAGTTAGCTGG	
Sdha (RefSeq: NM_023281.1)	FP: GGAACACTCCAAAAACAGACC	Eurofins genomics (MWG)
	RP: CCACCACTGGGTATTGAGTAGAA	
Tbp (RefSeq: NM_013684.3)	FP: CAGGAGCCAAGAGTGAAGAACA	Invitrogen Custom DNA Oligos
	RP: AAGAACTTAGCTGGGAAGCCC	

1337